



HAL
open science

Gold labelling of Green Fluorescent Protein (GFP)-tag inside cells using recombinant nanobodies conjugated to 2.4 nm thiolate-coated gold nanoparticles

Nadja Groysbeck, Mariel Donzeau, Audrey Stoessel, Anne Marie Haeberlé, Stéphane Ory, Danièle Spehner, Patrick Schultz, Ovidiu Ersen, Mounib Bahri, Dris Ihiawakrim, et al.

► To cite this version:

Nadja Groysbeck, Mariel Donzeau, Audrey Stoessel, Anne Marie Haeberlé, Stéphane Ory, et al.. Gold labelling of Green Fluorescent Protein (GFP)-tag inside cells using recombinant nanobodies conjugated to 2.4 nm thiolate-coated gold nanoparticles. *Nanoscale Advances*, In press, 10.1039/D1NA00256B . hal-03365147

HAL Id: hal-03365147

<https://hal.science/hal-03365147>

Submitted on 5 Oct 2021

HAL is a multi-disciplinary open access archive for the deposit and dissemination of scientific research documents, whether they are published or not. The documents may come from teaching and research institutions in France or abroad, or from public or private research centers.

L'archive ouverte pluridisciplinaire **HAL**, est destinée au dépôt et à la diffusion de documents scientifiques de niveau recherche, publiés ou non, émanant des établissements d'enseignement et de recherche français ou étrangers, des laboratoires publics ou privés.



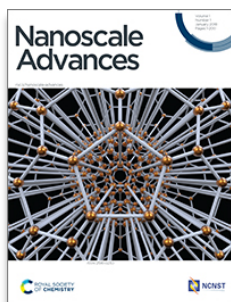
Gold labelling of Green Fluorescent Protein (GFP)-tag inside cells using recombinant nanobodies conjugated to 2.4 nm thiolate-coated gold nanoparticles

Journal:	<i>Nanoscale Advances</i>
Manuscript ID	NA-ART-04-2021-000256.R1
Article Type:	Paper
Date Submitted by the Author:	21-Jun-2021
Complete List of Authors:	Groysbeck, Nadja; Université de Strasbourg, CNRS UMR 7242 Donzeau, Mariel; Université de Strasbourg, UMR 7242 BSC Stoessel, Audrey; Université de Strasbourg, CNRS UMR 7242 Haeberlé, Anne Marie; CNRS, Institut des Neurosciences Cellulaires et Intégratives Ory, Stéphane; CNRS, Institut des Neurosciences Cellulaires et Intégratives Spehner, Danièle; IGBMC, 1, rue Laurent Fries Schultz, Patrick; IGBMC, 1, rue Laurent Fries Ersen, Ovidiu; University of Strasbourg, IPCMS Bahri, Mounib; Institut de physique et chimie des matériaux de Strasbourg, DSI Ihiawakrim, Dris; IPCMS Zuber, Guy; Université de Strasbourg, CNRS UMR7242

Nanoscale Advances

Guidelines for Referees

Thank you very much for agreeing to review this manuscript for [Nanoscale Advances](#).



Nanoscale Advances is an international gold open access journal, publishing good quality, reproducible new work across the breadth of nanoscience and nanotechnology that makes an important advance to the existing literature.

Articles should aim to publish good quality work that is discussed appropriately in the context of the literature.

The following manuscript has been submitted for consideration as a
PAPER

For acceptance, papers should report important field-advancing work that has not been published previously. Full papers based on Communications are encouraged provided that they represent a substantial extension of the original material. There are no restrictions on the length of a paper.

When preparing your report please:

- Focus on the **originality, importance, impact** and **reproducibility** of the science.
- Refer to the [journal scope and expectations](#).
- **State clearly** whether you think the article should be accepted or rejected and give detailed comments (with references) both to help the Editor to make a decision on the paper and the authors to improve it
- **Inform the Editor** if there is a conflict of interest, a significant part of the work you cannot review with confidence or if parts of the work have previously been published.
- **Provide your report rapidly** or inform the Editor if you are unable to do so.

Best regards,

Professor Chunli Bai

Editor-in-Chief, *Nanoscale Advances*

Professor Dirk Guldi

Editor-in-Chief, *Nanoscale Advances*

Dr Anna Rulka

Executive Editor, *Nanoscale Advances*

Contact us

Please visit our [reviewer hub](#) for further details of our processes, policies and reviewer responsibilities as well as guidance on how to review, or click the links below.



June 21st, 2021

Editor of Nanoscale advanced

Guy Zuber

Directeur de Recherche CNRS
Tél. +33 (0)3 68 85 47 68
mail : zuber@unistra.fr

Object: Submission of a revision of the manuscript "Gold immunolabeling of Green Fluorescent Protein (GFP)-tag inside cells using recombinant nanobodies conjugated to 2.4 nm thiolate-coated gold nanoparticles" for publication

Dear Editor

We would like to thank the reviewer for providing comments that help us correcting and improving our draft. The point-by-point answers to comments are listed below. The current submission includes correction in the main text and new sentences are highlighted as recommended.

We also modified images (Figures 4 and Figure 7) and included several new data, which are reported in the revised supporting information. The Figure 4 includes a quantification of size distribution as well as a HAADF-STEM image of the probe. The images B and C of Figure 7 were also modified for images that we found out of better quality than former ones.

REVIEWER REPORT(S):

Referee: 1

Comments to the Author

This manuscript describes the development of a novel probe based on non-covalent association of an anti-GFP nanobody and derivatised gold nanoparticle. The resulting probe shows great potential for localization of GFP-tagged proteins and the elegant system should be applicable to nanobodies against other targets, as they become available. The manuscript describes the development of the novel particles and presents a thorough characterization of their synthesis and testing, and an example of their potential use, with high precision localization in cells expressing GFP-tagged proteins.

Comments

- The advantages of this probe over existing reagents (such as antibody-gold reagents) is that the



nanobody can be synthesized in a reproducible fashion and has a specific known sequence, the nanobody-gold particle is very small, and using silver enhancement methods the size of the particle can be increased to allow simple electron microscopy (EM) or for detection by light microscopy. One possible drawback is the slightly variable stoichiometry but this is well-characterized in the manuscript and, as the authors point out, the multivalency can increase the avidity. One technical concern is that the only characterization of the clumping/crosslinking of the multivalent probe is by STEM (Figure 4) and no quantitation is provided. This issue should be examined more thoroughly.

Point to be addressed:

1. Characterization of the clumping/crosslinking and quantification issue (Figure 4)

Answer: The Figure 4 was modified to include a histogram reporting the distribution of sizes of the probe (e.g. the gold particle domain). The image is provided in Figure S7. The image displays 180 particles. Only 4 clusters were observed. Other fields (not shown) display the absence of clusters. To summarize these data, we added the following paragraph in the main text:

“The High-Angle annular dark field Scanning Transmission Electron Microscopy (HAADF-STEM) observation of (Nb-E3)₂:(K3)₂AuNP assemblies revealed gold particles of roughly spherical shape (Fig. 4 B). Analysis of a TEM image containing 180 gold particles (The sizes of the AuNP were distributed mostly between 2 and 2.6 nm TEM image containing 180 gold particles indicates that the diameters were mostly within the 2.0 to 2.6 nm range (average diameter: 2.31 nm; standard deviation: 0.31 nm) (Supporting information, Figure S7). Moreover, the image was almost devoid of clustered particles (less than 2%) indicating that the used synthetic condition mainly favours coordination of the two thiols of the bidentate K3 dimer onto gold atoms of one single AuNP, as drawn in the illustration (Figure 1).”

2. The main use of the probe is for pre-embedding labelling for EM, as shown in the manuscript. The examples presented use a protocol that is not compatible with good resolution EM (initial paraformaldehyde fixation and Triton X100 permeabilization). It would have been good to see how effective the probes can be with a protocol that minimizes cellular damage, for example an initial glutaraldehyde fixation and milder permeabilization protocol, as this would provide a practical example of its use in EM and the effective size of the particles in a real application where cellular preservation is optimal.

Answer: We did immunolabelling of GFP in 2%PFA, 0.02% glutaraldehyde fixed specimen. These data are now reported in the supporting information (Figures S9 and S10) and demonstrated the ability of the probe to detect GFP as well in glutaraldehyde fixed cells. We tried also 0.1% glutaraldehyde but we experienced silver staining of the control as well (eg the cell that was not incubated with gold particle). Weak coloration of the control was somehow also observed with the 2%PFA 0.02% glutaraldehyde fixed cells but never with 4%PFA (see Figures S9 and 10). We



therefore prefer to use 4% PFA as fixative on a first base. The following sentence and the reference 39 was added in the main text:

The ability of the $(\text{Nb-E3})_2:(\text{K3})_2\text{AuNP}$ to detect GFP in cellular specimen fixed with low percentage of glutaraldehyde³⁹ was preserved although with a lost in sharpness (Supporting information, Figures S9 and S10).

3. Have the authors tested the probes for on-section labelling for EM (eg. on thawed frozen sections or Lowicryl sections)? This would be another useful application as it would provide an alternative to commercial GFP antibodies.

Answer: no, we did not test these probes on thawed frozen section or lowicryl section due to time constraints. We feel confident that these probes will do the job as well for these applications since there are usefull for immunolabelling of glutaraldehyde fixed specimen.

4. In terms of the practicalities of the methods and their adoption by other groups, some details of the stability of the probes should be provided. Can the authors provide guidelines on storage of the final gold-nanobody particles or should the individual components be prepared and combined just before use?

Answer: we provided data on the stability of Nb-E3 (Figure S4) and guideline for storage. We include as well data showing that the full probe remain active after 7 days storage in the fridge. The $(\text{K3})_2\text{AuNP}$ was stored in the fridge and was still active 4 months after synthesis. We added this sentence in the material and method section:

“To note, the $(\text{K3})_2\text{AuNP}$ was stored at 4°C and was seen to remain stable for at least 4 months.”

Referee: 2

Comments to the Author

Molecular contrast in electron microscopy -- allowing localization of specific molecules in cellular electron microscopy -- is a major challenge. This manuscript addresses this long-standing major challenge. Described is an approach for gold labeling nanobodies that bind to Green Fluorescent Protein. The rationale (although not specifically stated) appears to be to enable Correlative Light - Electron Microscopy (CLEM)-- by imparting fluorescent contrast to tagged proteins for optical imaging and gold-cluster contrast to GFP for electron microscopy imaging. Much of what is reported is incremental. Gold cluster labeled nanobodies, labeled through Murray Place Exchange reactions were described in 2006 (reference 24, and a few other papers from Kornberg's lab -- e.g., Bioconjugate chemistry 21 (2), 214-218). It's really unclear why the dimerization domain from p53 is used-- why not just link directly to the nano body (as previously described in the Kornberg work).



Answer: we would have loved to be able to directly link the Nb to the AuNP using S-Au bond. However, we run in issues relative to lost of binding affinity and lost of integrity of protein. Passivation of the gold nanoparticle was also mandatory to minimize unspecific binding. The non-covalent method used in here provided a straightforward solution. We added the two sentences in the main text:

To work out a Nb-AuNP conjugate without loss of binding affinity of the Nb for its target and loss of protein integrity, we could have played around by comprehensive modification of the peptide sequence at the C-terminus. Instead of undergoing this classical approach, we chose to investigate a non-covalent functionalization approach using the properties of 2 peptides derived from the p53 protein to specifically form a stable heterotetramer composed of two homodimers (Figure 1).

We also added the following sentence in the main text as an other advantage of the non-covalent approach:

If the $(K3)_2$ AuNP is preferably mixed with the $(Nb-E3)_2$: right before use, the $(K3)_2$ AuNP complex was seen to remain active 7 days after storage at 4°C (Supporting Information, Figures S15). The selectivity of E3 dimer for the K3 dimer could also be exploited by detecting the specimen-bound $(GFP Nb-E3)_2$ with $(K3)_2$ AuNP through sequential incubations (Supporting Information, Figure S15).

It is very true for cellular work that smaller nanoparticle/antibody conjugates are desirable, since they will diffuse into fixed and permeabilized cells more effectively. This is also given as a motivation for the work. However, to this end, it would be really useful to compare the new construct presented in this work to FAB-NP or IgG-NP conjugates-- to show that the assertion is correct.

Answer: We linked the TAB, TNB AuNB to a monoclonal mouse anti-GFP antibody and evaluate its ability to label GFP-protein with gold in H2B HeLa cells (Figures S11 to S14). The following sentence was added in the main text to summarize results of experiments:

For comparison of labelling activity, a mouse anti-GFP antibody-gold particle conjugate made from the same TAB-, TNB- coated gold particle and a monoclonal 150 kDa IgG was prepared (Supporting Information, Figure S11). Its gold labelling ability was similar to the one of $(Nb-E3)_2:(K3)_2$ AuNP (Supporting Information, Figures S12-S14). A tendency of the anti-GFP IgG-AuNP conjugate to preferentially label the nuclear periphery of the H2B-GFP HeLa was noticed (Figures S12 and S14).

Ultimately the authors have to silver-enhance the 2.4nm gold particles in order to see them in the EM of cells. It'd be interesting for the authors to compare this to Leapman's prior work in imaging gold nanoparticles in cells, where smaller particles than the ones used here could be viewed in HAADF-STEM mode. Small 8 (14), 2277-2286



Answer: We do not wish to compare our work to Leapman's prior work as it is not the main focus of our manuscript. We were actually able to see 2.4 nm particles inside the cell nucleus using HAADF-STEM in a work analogous to Leapman's study. We permeabilize living HeLa cells by electroporation to allow the entry of 2.4 nm particle inside cells. We were able to detect the particle inside the cell after silver enhancement but also without silver enhancement using HAADF-STEM. It was challenging but occurrence of aggregated AuNPs as seen in Leapman's images) help us to zoom in the "good" area/spot. In the immunolabelling case, most particles (if not all) are individual. It does indicate probe of excellent quality: however this behavior does not facilitate detection of the "good" spot containing the cells. We will keep on trying but we also have to manage with access to facility and cost of use.

The manuscript does show correlative imaging of HeLa cell sections where β -Gal-GFP), Mitochondria-Targeting Signal tagged GFP (MTS-GFP), GFP tagged-PCNA- Interacting Peptide (GFP-PIP), and H2B-GFP are imaged. This is on the one hand definitely showing things that haven't been seen before (great!), and on the other hand, showing that with silver enhancement, you don't really get better resolution than you can get in optical microscopy -- therefore why do the electron microscopy work at all (or -- tell the reader what additional information is gained in the EM micrographs compared to the light microscope micrographs -- which are much easier to acquire.)

Overall -- the paper should be improved before publication in Nanoscale Advances. The improvement could be in one of the following areas:

1. Data that compares the efficacy of the nano body constructs to more commonly used FAB or IgG constructs -- testing the hypothesis that smaller is better in this case.

Answer: We linked the TAB, TNB AuNP to a monoclonal mouse anti-GFP antibody and evaluate its ability to label GFP-protein with gold in H2B HeLa cells (Figures S11 to S14). As seen the synthetic procedure is straightforward as well but implies a sequential procedure in where the Ab the initial "substrate". The following sentence was added in the main text to summarize results of experiments:

"For comparison of labelling activity, a mouse anti-GFP antibody-gold particle conjugate made from the same TAB-, TNB- coated gold particle and a monoclonal 150 kDa IgG was prepared (Supporting Information, Figure S11). Its gold labelling ability was similar to the one of (Nb-E3)₂:(K3)₂AuNP (Supporting Information, Figures S12-S14). A tendency of the anti-GFP IgG-AuNP conjugate to preferentially label the nuclear periphery of the H2B-GFP HeLa was noticed (Figures S12 and S14)."



2. Interpretation of data in a way that shows the utility of this approach (how does it give more information than one gets in an optical micrograph)?

Answer: We modify the conclusion to indicate that these probe are useful using two imaging modalities

More minor concerns:

3. Fig4B is HRTEM, not STEM. If they used a Cs-corrected JEOL-2100F, they should absolutely be able to get a better image than F7C.

Answer: The Figure 4 was modified. It displays a HAADF-STEM of the probe as well as size distribution of a representative population of particles

4. I recommend EDS work with Ag-enhancement to see if particulate would form where gold is and is not located. It's straightforward to do a point-and-shoot spectrum.

Answer: An EDX analysis of the nuclear portion containing contrasting particles was performed (See supporting information Figure S17). The spectrum shows the presence of the gold and silver atoms confirming the assertion from Aurion about selective deposition of silver onto AuNPs.

Sincerely yours

Guy Zuber

ARTICLE

Gold labelling of Green Fluorescent Protein (GFP)-tag inside cells using recombinant nanobodies conjugated to 2.4 nm thiolate-coated gold nanoparticles

Received 00th January 20xx,
Accepted 00th January 20xx

DOI: 10.1039/x0xx00000x

Nadja Groysbeck,^a Mariel Donzeau,^a Audrey Stoessel,^a Anne-Marie Haeberle,^b Stéphane Ory,^b Danièle Spehner,^c Patrick Schultz,^c Ovidiu Ersen,^d Mounib Bahri,^d Dris Ihiwakrim,^d Guy Zuber^{a*}

The advances in the microscopy technology have prompted efforts to improve the reagents required to recognize specific molecules within the intracellular environment. For high-resolution electron microscopy, conjugation of selective binders originating from the immune response arsenal to gold nanoparticles (AuNPs) as contrasting agents is the method of choice to obtain labeling tools. However, conjugation of the minimal sized 15 kDa nanobody (Nb) to AuNP remains challenging in comparison to the conjugation of 150 kDa IgG to AuNP. In here, effective Nb-AuNP assemblies are built using the selective and almost irreversible non-covalent associations between two peptide sequences deriving from a p53 heterotetramer domain variant. The 15 kDa GFP-binding Nb is fused to one dimerizing motif to obtain a recombinant Nb dimer with improved avidity for GFP while the other complementing dimerizing motif is equipped with thiols and grafted to a 2.4 nm substituted thiobenzoate-coordinated AuNP via thiolate exchange. After pegylation, the modified AuNPs are able to non-covalently anchor Nb dimers and the subsequent complexes demonstrate the ability to immunogold label GFP-protein fusions within various subcellular locations. These tools open an avenue for precise localization of targets at high resolution by electron microscopy.

1. Introduction

The investigation of protein trafficking and localization is fundamental to understand cell functioning. Fluorescent microscopy (FM) and Electron Microscopy (EM) are two valuable tools in this endeavour.¹ Continuous technological advances in both FM and EM are steadily pushing the resolution boundaries and providing new insights on how cellular constituents precisely organize together and participate in the life and wellbeing of biological organisms. Pinpointing selected elements within the subcellular organization is unfortunately not always feasible due to the lack of contrast differential between the various cellular constituents. Specific labelling methodologies must therefore be developed and optimized to accompany the progress of microscopy technology. The *Aequorea victoria* Green Fluorescent Protein (GFP) and fluorescent derivatives are popular tags to label chosen proteins through genetically

made fusion proteins and to localize them with FM even in living cells and organisms. For EM, gold nanoparticles (AuNPs) are the contrasting agents of choice.² The traditional AuNP-antibody conjugates first reported by Faulk and Taylor,³ consisting of 150 kDa antibodies that are physically adsorbed onto colloidal AuNPs of 10-15 nm, are still in use today. Yet, the large size of AuNPs and IgG molecules, as well as the difficult to define bonds between the AuNP and the IgG hamper the efficiency of labelling as well as accurate target localization.⁴ Reduction of the AuNP's diameter to less than 1.4 nm led to improved labelling agents with favourable diffusion and penetration abilities into tissues.⁵ Replacement of the full 150 kDa IgG with the smaller 50 kDa fragment antigen-binding domain (Fab) was also beneficial.^{6,7} In a step toward further optimization, 12-15 kDa single-domain camelid antibody fragments (VHH) or nanobodies (Nbs) appear highly appealing.⁸⁻¹⁰ They are interesting not only because of their compactness (molecular weight (MW) of ca. 15 kDa for a size of 4 nm x 2.5 nm), but also due to their bioengineering properties.¹¹ Point mutations of selected amino-acids to cysteines^{12,13} afford precise attachment sites for thiol-reactive fluorophores. The resulting fluorescently-labelled Nbs have known spacing distances between the targeted epitope and the fluorescent signal,¹⁴ affording probes with enhanced target localization accuracy suited for super-resolution microscopy imaging of biological targets.^{15,16} Nanobodies have also been applied to EM immunolabelling.

^a Université de Strasbourg – CNRS, UMR 7242 Laboratoire de Biotechnologie et Signalisation Cellulaire, Boulevard Sébastien Brant, 67400 Illkirch, France.

^b Centre National de la Recherche Scientifique, Université de Strasbourg, Institut des Neurosciences Cellulaires et Intégratives, F-67000 Strasbourg, France.

^c Université de Strasbourg – Department of Integrated Structural Biology, Institut de Génétique et de Biologie Moléculaire et Cellulaire, 67400 Illkirch, France

^d Université de Strasbourg – CNRS, UMR 7504, Institut de Physique et Chimie des Matériaux de Strasbourg (IPCMS) 23 rue de Loess, 67034 Strasbourg, France.

* zuber@unistra.fr

Electronic Supplementary Information (ESI) available: Additional experimental protocols and Data . See DOI: 10.1039/x0xx00000x

ARTICLE

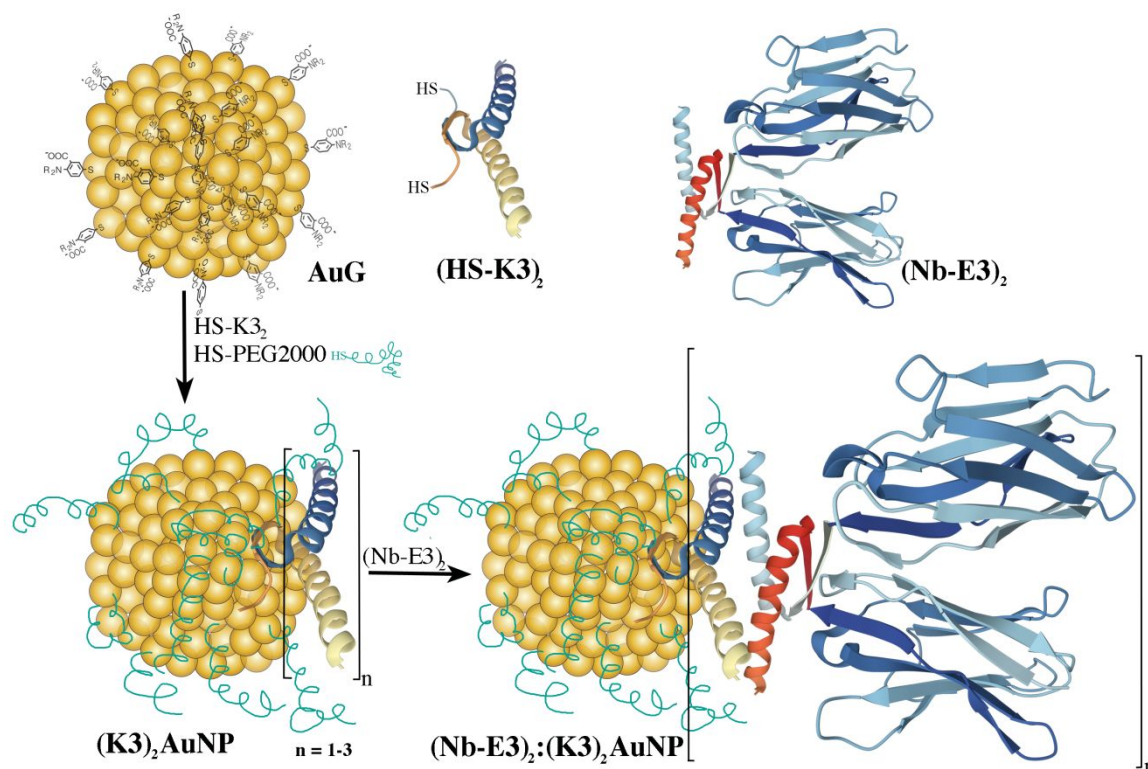


Figure 1. Schematic route for the synthesis of the Nb₂-AuNP conjugates using the strong and mutual associating ability of E3 and K3 dimers originating from a p53 heterotetramer.^{17,18} According to the structure of the p53 tetramerization domain (pdb1OLG),¹⁹ the dimers mainly fold into α -helices. The GFP binding nanobody (Nb) mainly folds into β -sheets (in blue pdb30GO).²⁰

Kijanka and colleagues developed a protocol for the labelling of HER2 using an HER2 binding Nb followed by a secondary anti-Nb antibody and then a protein A-gold particle conjugate.²¹ Ariotti and colleagues developed fusion proteins between GFP-binding Nbs and a soybean ascorbate peroxidase to locally produce a stain upon addition of diaminobenzidine (DAB) and H₂O₂.^{22,23} The brownish stain visible by optical microscopy (OM) could be further converted into an electron dense product through treatment with OsO₄, permitting correlative light and electron microscopy observation. Investigation of the direct conjugation of Nbs to 10–15 nm AuNPs by adsorption has been reported by Goossens and colleagues.²⁴ Functional conjugates were obtained but maintaining the colloidal stability of the nanobody-AuNP conjugates was clearly extremely challenging because of the huge difference in bulkiness between the Nb and the AuNP. Decreasing the difference can be achieved by decreasing the diameter of the AuNP.²⁵ However, decreasing the diameters weakens the strength of protein adsorption onto the AuNP surface, leading to highly dynamic protein coronas.^{26,27} If the gold-bound protein layer is mandatory for target recognition, linkage of the protein to the AuNP should hence be performed

using stronger coordination links such as the Au-S bonds^{28,29} and/or functionalization strategies involving covalent bonds.³⁰ To design Nb-AuNP conjugates with usefulness for gold immunolabelling application of cellular specimen, we explored methods for strongly linking thionitrobenzoates-coated AuNPs (AuG)^{31,32} to bioengineered GFP binding Nbs.^{8,20} We discovered that the non-covalent conjugation approach based on the complementary associating dimers originating from a p53 heterotetramer variant,^{17,18,33} led to Nb:AuNP assemblies with excellent immunogold labelling abilities (Figure 1).

2. Results and discussion

2.1 Synthesis of GFP nanobody-AuNP conjugate

To generate immunogold probes based on Nbs, we selected the GFP binding Nb cAbGFP4 with a previously determined structure. It displays a dissociation constant (K_d) within the nanomolar range.²⁰ For the gold domain, we used the 2.4 nm AuG that was previously described and extensively characterized.³²

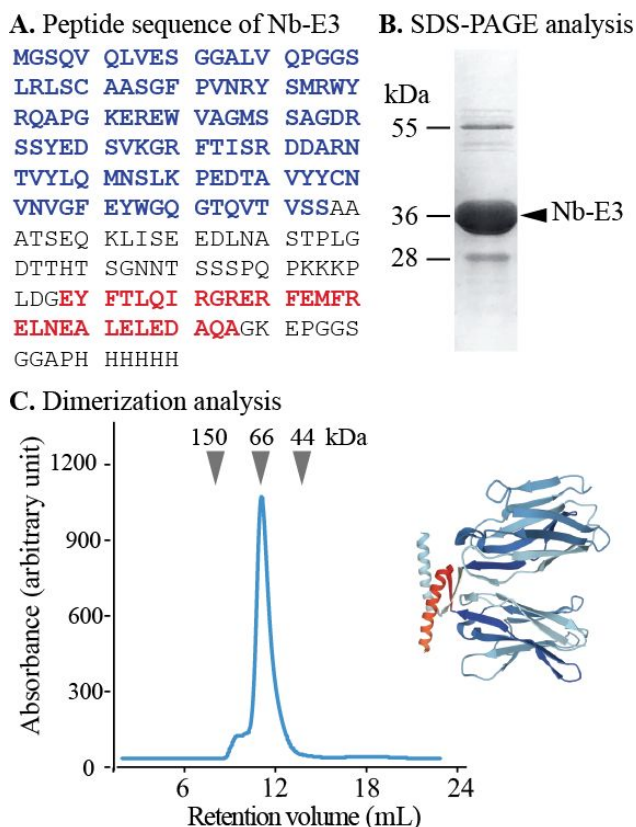


Figure 2. Characterization of the recombinant E3 tagged GFP binding nanobody. A. Peptide sequence. The GFP VHH (blue) is fused to the E-enriched p53 oligomerization domain (red) and to a polyhistidine tag. B. SDS PAGE analysis of the bacteria-expressed and purified protein after Ni-NTA chromatography showed monomeric Nb-E3. C. Size exclusion chromatography of the purified E3-fused nanobody. Elution of a species with an apparent molecular weight of 66 kDa confirmed dimerization.

This AuG is water-soluble and contains a single layer of substituted thiobenzoates that can be readily replaced with other thiol-containing molecules via a thiolate-for-thiolate exchange. Functionalized AuNPs with robust Au-S coordination bonds might hence be conveniently synthesized.

In our first attempts, we investigated the preparation of nanobody-AuNP conjugates directly from Nbs that were point-mutated to contain an additional thiol.¹⁴ The GFP binding Nb sequence was bioengineered to possess either a C-terminal cysteine (C143-Nb) or a cysteine at the position 7 (C7-Nb). The C143-Nb displayed **severe** proteolytic instability and was not further used (Supporting Information, Figure S1). The C7-Nb was stable at 4°C for more than six months, had GFP binding ability similar to that of the wild type Nb (Supporting Information, Figure S2) and could be linked to AuG via Au-S coordination. The conjugates could be further purified and characterized by SDS-PAGE (Supporting Information, Figure S3). **Unfortunately, in contrast to the covalent appending of fluorescent molecules,**¹⁴ the **direct** coordination of C7-Nb onto the **2.4 nm** AuNP dramatically altered its ability to bind GFP and labelling potency (Figures S3). The direct Au-S coordination bond at this C7 position may have exposed the nanobody to the AuNP's corona, resulting in obliteration of the nearby GFP-Nb binding interface.

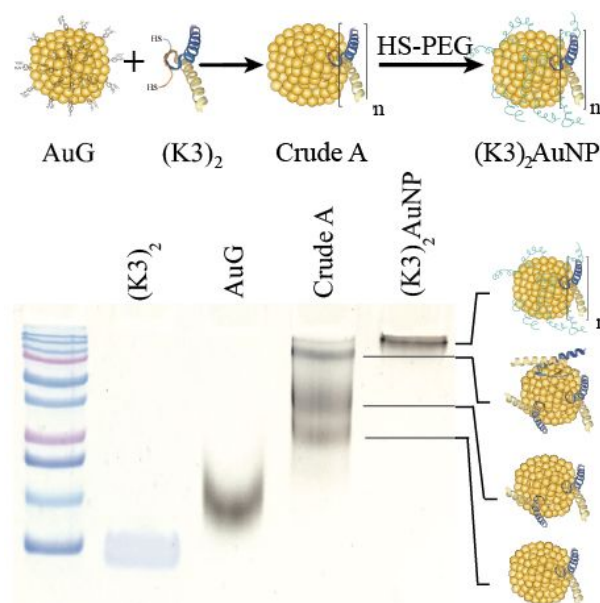


Figure 3. PAGE analysis of reaction products obtained by reaction of AuG with 3 molar equivalent of thiolated K3 dimer (Crude A) and then thiolated PEG 2000 Da ((K3)₂AuNP).

Such alteration of the Nb specificity for its target after conjugation has already been pointed out in the literature.¹⁰ Even the functionalization of Nbs with fluorophores of M.W. smaller than 1000 Da fluorophores via random coupling to lysines can drastically reduce Nb binding.¹⁴

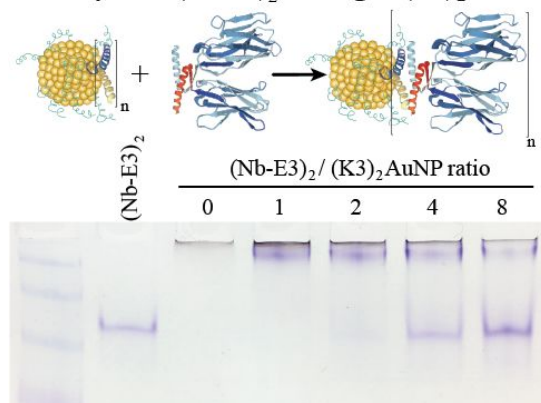
To work out a Nb-AuNP conjugate without loss of binding affinity of the Nb for its target and loss of protein integrity, we could have played around by comprehensive modification of the peptide sequence at the C-terminus. Instead of undergoing this classical approach, we chose to investigate a non-covalent functionalization approach using the properties of 2 peptides derived from the p53 protein to specifically form a stable heterotetramer composed of two homodimers (Figure 1). Relative to the native p53 tetramerization domain, one sequence was enriched in lysine (K) while replacement of one K with glutamic acid (E) provided a E-enriched sequence (E3).¹⁷ These E- and K-enriched sequences, named E3 and K3 respectively, were recently demonstrated to conveniently favour the selective non-covalent union of 2 distinctly tagged functional proteins into highly stable heterotetramers even in complex biological fluids crowded with all sorts of proteins and diverse compounds.^{18,33}

First, the Nb was genetically engineered at its C-terminal end with the aspartate-enriched variant of the p53 heterotetramer domain (E3) along with a polyhistidine sequence (Figure 2).¹⁸ The recombinant Nb-E3 fusion protein was then produced in *E. coli* and purified by immobilized metal affinity chromatography followed by size exclusion chromatography (SEC) with high yield and purity (Figure 2B). The SEC profile showed elution of a species with an apparent Molecular Weight (MW) close to 66 kDa corresponding to the MW of a dimer of Nb-E3 (Figure 2C). The integrity of the Nb-E protein was fully maintained upon storage at -80°C. Proteolytic cleavage was nonetheless

observed upon storage > 120 days at 4°C (Supporting information, Figure S4).

The K3^{17,18} was fused to the CALNN motif.³⁴ According to extrapolation from the structure of the p53 domain,¹⁹ the two cysteines at the N-terminal end are 2 nm apart with little chance to cross react. They can also point toward the same direction, offering possible bidentate coordination to AuG upon thiolate exchange reaction. Functionalization of the AuG with this dimer in 0.1 M HEPES buffer, pH 7.5 was then assayed at increasing dimer/AuG ratios (Supporting Information, Figure S5). After a 3h incubation time at 25°C to allow thiolate-to-thiolate exchange of Au(I)-coordinated ligands on the AuG surface, the crude reactions were analysed by SDS-PAGE. Functionalization of the AuNP with the dimer via exchange of ligands proceeded smoothly with an increased number of dimer attachment per particle by increasing the dimer/AuG ratios. At the dimer/AuG ratio of 3, the mixture was devoid of unreacted AuG. Three distinctive AuNP species with different electrophoretic mobility were produced, likely corresponding to AuNPs equipped with 1, 2 and 3 dimers. To note, the masking of the gold surface of AuG by coordination of thiolated PEG 2000 Da was mandatory to minimize non-specific adsorption of the probe onto cellular ultrastructure (Supporting Information, Figure S6). Therefore, this reaction condition was scaled-up and immediately followed by the addition of excess thiolated PEG 2000 Da to ensure full PEG-mediated shielding of the AuNP surface (Figure 3). The end product (K3)₂AuNP, barely migrated into the polyacrylamide gel, likely because of the properties of PEG to shield the superficial charge of nanomaterial.^{35,36}

A. Analysis of (Nb-E3)₂ binding to (K3)₂AuNP



B. HAADF-STEM of (Nb-E3)₂:(K3)₂AuNP

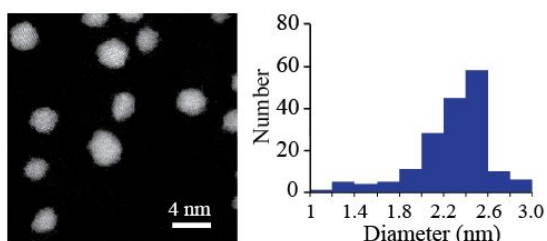


Figure 4. Characterization of the non-covalent (Nb-E3)₂:(K3)₂AuNP assemblies. A. Native PAGE analysis to determine the average stoichiometry for complete assembly of (Nb-E3)₂ with (K3)₂AuNP. B. Scanning Transmission Electron Microscopy (STEM) analysis of the (Nb-E3)₂:(K3)₂AuNP.

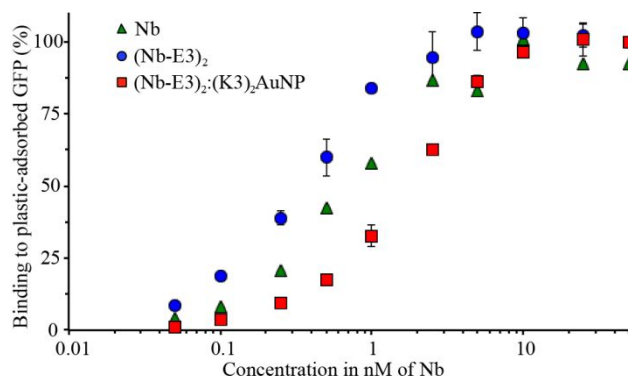


Figure 5. Apparent binding abilities of the GFP-binding nanobody (green triangle), the dimerized (Nb-E3)₂ (blue dot) and the non-covalent (Nb-E3)₂:(K3)₂AuNP assemblies (red square). The binding to GFP was determined using indirect ELISA analysis and plate-adsorbed GFP

The non-covalent association of (Nb-E3)₂ to (K3)₂AuNP was next evaluated by titrating the (K3)₂AuNP PAGE with increasing amounts of (Nb-E3)₂. A PAGE analysis in non-denaturing conditions allowed the assessment of binding by detecting free/unbound (Nb-E3)₂ (Figure 4). A small amount of free (Nb-E3)₂ started to be detected at the (Nb-E3)₂:(K3)₂AuNP ratio of 2 indicating that each (K3)₂AuNP can anchor slightly less than 2 (Nb-E3)₂. In the next experiments, the non-covalent (Nb-E3)₂:(K3)₂AuNP assemblies were generated by mixing the modified AuNP with 2 molar equivalents of (Nb-E3)₂.

The High-Angle annular dark field Scanning Transmission Electron Microscopy (HAADF-STEM) observation of (Nb-E3)₂:(K3)₂AuNP assemblies revealed gold particles of roughly spherical shape (Fig. 4 B). Analysis of a TEM image containing 180 gold particles (The sizes of the AuNP were distributed mostly between 2 and 2.6 nm TEM image containing 180 gold particles indicates that the diameters were mostly within the 2.0 to 2.6 nm range (average diameter: 2.31 nm; standard deviation: 0.31 nm) (Supporting information, Figure S7). Moreover, the image was almost devoid of clustered particles (less than 2%) indicating that the used synthetic condition mainly favours coordination of the two thiols of the bidentate K3 dimer onto gold atoms of one single AuNP, as drawn in the illustration (Figure 1).

2.2 Binding ability of non-covalent (Nb-E3)₂:(K3)₂AuNP to GFP

In order to use the complex as a probe for GFP in microscopy, we had to check whether the (Nb-E3)₂:(K3)₂AuNP complex maintained its ability to bind GFP. To do so, we performed an indirect ELISA assay using purified GFP as the plastic-immobilized antigen and compared the binding profiles of the wild type Nb, (Nb-E3)₂ and (Nb-E3)₂:(K3)₂AuNP complex (Figure 5). The dose-dependent binding of the various Nbs tested showed similar sigmoidal profiles from which we assessed the apparent K_ds. Accordingly, we found a K_d of 0.8 nM for the wild type Nb, 0.4 nM for each Nb of (Nb-E3)₂ and 2 nM for each Nb of (Nb-E3)₂:(K3)₂AuNP.

ARTICLE

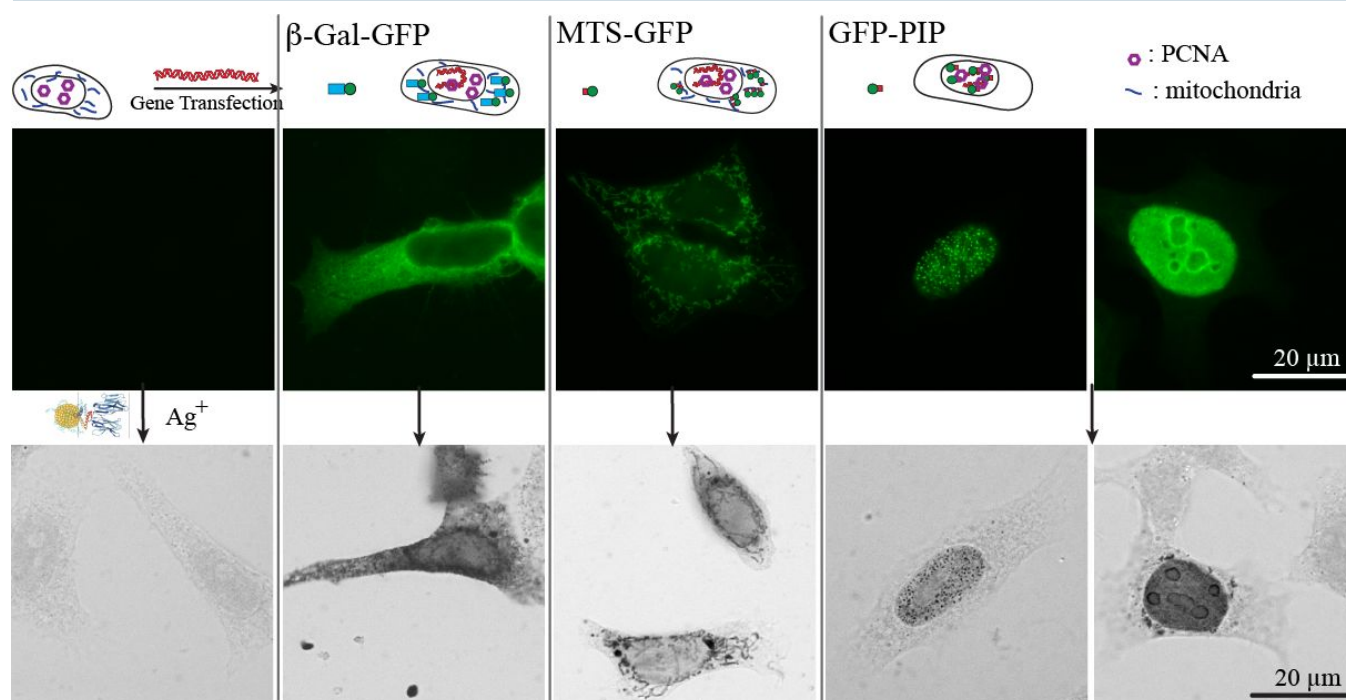


Figure 6. Fluorescent and (Nb-E3)₂:(K3)₂AuNP-mediated detection of protein-GFP fusions after transient gene transfection. HeLa cells were transiently transfected with DNA plasmids to express different GFP-protein fusions as indicated: β -Galactosidase-GFP (β -Gal-GFP), Mitochondria-Targeting Signal tagged GFP (MTS-GFP), GFP tagged-PCNA-Interacting Peptide (GFP-PIP). Upper images: Detection of the GFP signal in PFA-fixed HeLa cells 24 hours after DNA plasmid transfection. Lower images: the cell membrane was permeabilized, the cells were incubated with 6 nM (Nb-E3)₂:(K3)₂AuNP, washed and the gold nanoparticles bound to cellular components were detected by extensive silver enhancement visible by BFM

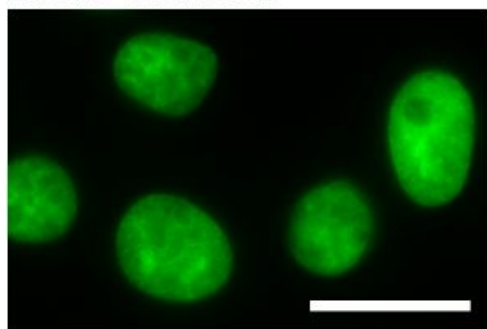
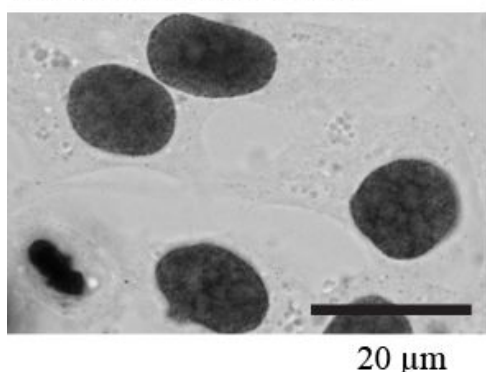
The K_d values indicated that the E3-mediated dimerization of Nb results in a gratifying avidity effect (four fold increased in apparent affinity when the (Nb-E3)₂ is compared to Nb).^{18,37} In contrast, the grafting of about 2 (Nb-E3)₂ onto (K3)₂AuNP resulted in a 5-fold affinity loss relative to the (Nb-E3)₂.

The reason behind the apparent affinity loss of (Nb-E3)₂ after anchorage to the (K3)₂AuNP might be explained by the presence of the PEG. The PEG is required to minimize unspecific association of proteins to the AuNP surface. However, its bulkiness and vicinity to the Nb-anchored AuNP may entail a weakening of the apparent binding affinity of the AuNP-attached nanobodies for GFP.

The efficiency of the (Nb-E3)₂:(K3)₂AuNP complex to mark GFP-protein fusions with a AuNP inside cells was then evaluated using immunocytochemistry method followed by bright field microscopy (BFM) (Figure 6). HeLa cells were transiently transfected with DNA plasmids encoding a β -Galactosidase-GFP (β -Gal-GFP), a Mitochondria-Targeting Signal tagged GFP (MTS-GFP) and a GFP tagged-PCNA-Interacting Peptide (PIP) (GFP-PIP). The cells expressing various levels of each exogenous protein were then observed by FM (Figure 6, upper images). The subcellular localization of these GFP-protein fusions were then assayed by immunogold labelling

with (Nb-E3)₂:(K3)₂AuNP followed by silver enhancement to sizes observable by BFM (Figure 6, lower images). Comparison between the FM and BFM images of the transfected HeLa cells showed an excellent correlation between the fluorescent signal and the silver-enhanced AuNPs. The 520 kDa β -galactosidase-GFP fusion protein was seen inside the cytosol but not inside nuclei in agreement with the function of the nuclear envelop to block passive diffusion of macromolecules above 50 kDa. When the 520 kDa β -galactosidase-GFP fusion was further equipped with a Nuclear Localization Signal (NLS), FM and immunogold labelling experiments showed also the expected transport of β -Gal-GFP-NLS into the cell nuclei (Supporting Information, Figure S8). The preferential accumulation of MTS-GFP in mitochondria (filamentous ultrastructure near surrounding the nucleus) was also observed by the immunogold labelling protocol. The GFP-PIP can be used as a marker for cell replication.³⁸ Two patterns could be observed in transfected cells: GFP-PIP fluorescent foci in the nucleus corresponding to early DNA replication initiation sites, or the nucleus filled with GFP-PIP with accumulation near the nucleoli corresponding to a more advanced state of DNA replication. Both of these patterns were also observed using (Nb-E3)₂:(K3)₂AuNP.

A. H2B-GFP HeLa

B. H2B-GFP HeLa labeled with $(\text{Nb-E3})_2:(\text{K3})_2\text{AuNP}$ 

C. HAADF-STEM of gold labeled H2B-GFP HeLa

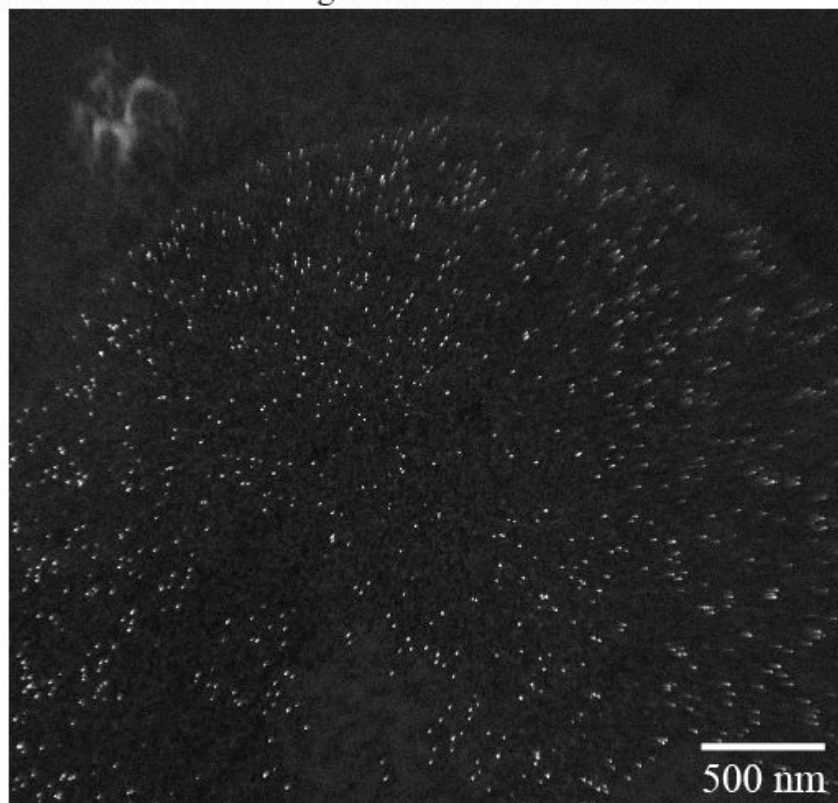


Figure 7. Fluorescent and $(\text{Nb-E3})_2:(\text{K3})_2\text{AuNP}$ -mediated detection of H2B-GFP fusions inside the nuclei of HeLa cells transformed to stably express H2B-GFP fusions. A. Fluorescence detection of GFP in H2B-GFP HeLa. B. BFM image of H2B-GFP HeLa with $(\text{Nb-E3})_2:(\text{K3})_2\text{AuNP}$ and extensive silver enhancement. C. HAADF-STEM image of H2B-GFP HeLa after labelling with $(\text{Nb-E3})_2:(\text{K3})_2\text{AuNP}$ and mild silver enhancement.

The ability of the $(\text{Nb-E3})_2:(\text{K3})_2\text{AuNP}$ to detect GFP in cellular specimen fixed with low percentage of glutaraldehyde³⁹ was preserved although with a loss in sharpness (Supporting information, Figures S9 and S10). For comparison of labelling activity, a mouse anti-GFP antibody-gold particle conjugate made from the same TAB-, TNB- coated gold particle and a monoclonal 150 kDa IgG was prepared (Supporting Information, Figure S11). Its gold labelling ability was similar to the one of $(\text{Nb-E3})_2:(\text{K3})_2\text{AuNP}$ (Supporting Information, Figures S12-S14). A tendency of the anti-GFP IgG-AuNP conjugate to preferentially label the nuclear periphery of the H2B-GFP HeLa was noticed (Figures S12 and S14). If the $(\text{K3})_2\text{AuNP}$ is preferably mixed with the $(\text{Nb-E3})_2$: right before use, the $(\text{K3})_2\text{AuNP}$ complex was seen to remain active 7 days after storage at 4°C (Supporting Information, Figures S15). The selectivity of E3 dimer for the K3 dimer could also be exploited by detecting the specimen-bound $(\text{GFP Nb-E3})_2$ with $(\text{K3})_2\text{AuNP}$ through sequential incubations (Supporting Information, Figure S15). Altogether, the experiments clearly demonstrate the usefulness of $(\text{Nb-E3})_2:(\text{K3})_2\text{AuNP}$ as probe to label GFP and fusion proteins with gold particles either inside the cytosol or inside the nucleus.

2.3 $(\text{Nb-E3})_2:(\text{K3})_2\text{AuNP}$ assemblies for immunogold labelling of GFP-protein fusion inside cells by Electron Microscopy

We next evaluated whether $(\text{Nb-E3})_2:(\text{K3})_2\text{AuNP}$ complexes were suitable for EM labelling of GFP-tagged proteins in cells using a stably transformed HeLa cell line that expresses the nuclear histone protein H2B fused to GFP.⁴⁰ First, the stable H2B-GFP HeLa and wild type HeLa cell lines were fixed and permeabilized for immunocytochemistry labelling with extensive silver-mediated amplification of AuNPs for FM and BFM imaging (Figure 7, Images A and B). Since the silver staining correlated well with the GFP signal, the cells were processed for gold immunolabelling and moderate silver enhancement before resin embedding, sectioning and EM observation of the specimen. We also prepared an EM specimen of the immunolabelled HeLa H2B-GFP without the silver enhancement step. This non-silver enhanced specimen was analysed for gold content in the nucleus using Energy Dispersive X-ray (EDX) spectroscopy (Supporting Information, Figure S16). The EDX spectrum clearly demonstrated the presence of gold atoms inside the cell nucleus ($\text{Au}_{\text{Ma}} = 2.123 \text{ keV}$, $\text{Au}_{\text{Mb}} = 2.203 \text{ keV}$, $\text{Au}_{\text{La}} = 9.713 \text{ keV}$, $\text{Au}_{\text{Lb}} = 11.443 \text{ keV}$). Unfortunately, in our hands, the direct visualization of the AuNPs in the cell sections was unfruitful for the moment due to the low contrast of the specimen and

difficulty to find the nucleus in where to zoom in. We therefore performed a mild silver enhancement procedure of the specimen containing (Nb-E3)₂:(K3)₂AuNP-labeled H2B-GFP HeLa cells to grow the size of the particle to size below 20 nm. After sectioning, the specimen was analysed by TEM. HAADF-STEM (Figure 7, image C) clearly showed the presence of discrete particles inside the nucleus. EDX spectroscopy confirmed that these particles were composed of silver and gold (Supporting Information, Figure S17). The density of AuNPs in the different subcellular compartments was then measured by compiling data from six images to obtain: 37 AuNPs per μm^2 in the heterochromatin (HC) near the nuclear periphery; 14 AuNPs per μm^2 within the perinucleolar compartment (PC) and; 4 AuNPs per μm^2 within the euchromatin (EC) regions within the nucleus. The nucleoli and the cytosol were almost devoid of probes (0.5 and 0.2 AuNPs per μm^2 for the Nucleoli and cytosol, respectively). A similar H2B-GFP nuclear labelling pattern was also obtained using conventional TEM whereas the wild type HeLa was devoid of any particles (Supporting Information, Figure S18). A preferential localization of H2B-GFP in the heterochromatin near the nuclear or nucleolar periphery was in agreement with published studies.^{40,41} We can nonetheless note a discrepancy between nuclear staining seen by OM and inhomogeneous nuclear labelling observed by EM. This variation likely results from the silver staining procedure (sizes of AuNP-seeded silver particles for BFM imaging were made larger than the ones for EM imaging) and from the difference in specimen thickness (BFM images were projections of light intensity variation throughout the whole cell; EM were performed on about 100 nm thick specimen). The density of gold labelling inside the nuclei was lower than the expected calculated density of nearly 10^4 H2B per μm^2 (one human cell nucleus contains approximately 30 million nucleosomes, corresponding to 60 million H2B molecules).⁴² However, the immunogold labelling protocol often underestimates the real number because PFA might preclude recognition of a proportion of target epitope. High local concentration of targets might also play a role.⁴³ In our specific case, the H2B-GFP fusion was moreover expressed in addition to the endogenous non-labelled H2B, likely at a low percentage.

3. Materials and methods

3.1 Genetic engineering of the Nb-E3 construct

The GFP binding nanobody was engineered to contain the E3 peptide sequence¹⁸ and polyhistidine at the C terminal end. The GFP binding nanobody²⁰ gene was amplified using PCR and primers of sequences: CGTCAG CCATGG GGTCCC AGGTTTCAGC and CCACAG GAATTC ACAATG GTGATG ATGGTG ATGTGCG. The DNA fragment was then inserted into a pETOM vector containing the E3 tag DNA sequence using *NcoI* and *SpeI* restriction sites.¹⁸

3.2 Expression and purification of (Nb-E3)₂

The Recombinant nanobody was expressed in *E. coli* BL21(DE3)pLys after induction with 1 mM IPTG in 100 mL LB medium at 20°C for 24h. The bacteria were lysed by ultrasonication. The his-tagged proteins were then purified by immobilized metal affinity chromatography using a HisTrap HP column (1 mL) charged with NiSO₄ and then by gel filtration on a HiLoad Superdex 200PG preparative column operating at a flow rate of 0.5 mL/min. Protein fractions were analysed by SDS-PAGE. Selected fractions were pooled and protein solutions were concentrated with Amicon Ultra 4 mL centrifugal devices (MWCO 3 kDa).

3.3 Synthesis of AuNP-nanobody conjugates

Typically, the AuG in 0.1 M HEPES, pH 7.5 solution (70 μL , 3 nmol) was added to the peptide of sequence [CALNNGEYFTLQIRGRERFEMFRKLNKALELKDAQA] (176 μL of a 1 mM solution, 18 nmol) freshly prepared in 0.1 M HEPES, pH 7.5. After 3 h at 25°C the remaining exchangeable thiolates on the AuG surface were then exchanged to polyethyleneglycol 2000 Da by addition of alpha-methoxy-omega-mercapto poly(ethylene glycol) 2000 Da (276 μL of a 1 mM solution, 276 nmol) followed by a 3h incubation time at 25°C. The crude mixture was then purified by ultrafiltration (30 kDa cut-off) (5 times 0.5 mL of 0.1 M HEPES, pH 7.5) to yield 50 μL of the modified AuNP ((K3)₂AuNP). The concentration of AuNP was determined spectrophotometrically to be 18 μM .^{44,45} The (Nb-E3)₂:(K3)₂AuNP was finally obtained by addition of (Nb-E3)₂ (20 μL of a 5 μM solution, 100 pmol) with the (K3)₂AuNP (5 μL of a 10 μM solution).

3.4 Transfection experiments

The plasmids encoding Mitochondria Targeting Signal-GFP fusion (MTS-GFP), GFP- β -galactosidase fusion (GFP- β -gal), GFP-PCNA Interacting Peptide fusion (GFP-PIP) were gifts from Prof. Étienne Weiss and Dr. Mariel Donzeau.⁴⁴ They were transfected into HeLa cells using PEI derivatives.^{46,47} Cells were seeded onto glass coverslips in 24-well plates at 50000 cells/well the day before the transfection experiment. Transgene expression was analysed after 24 h.

3.5 Immunocytochemistry for bright field microscopy

Coverslip-adhered cells were fixed with 4% PFA in PBS for 20 min at 20°C. The coverslips were then washed with PBS (3 x 0.5 mL, 5 min), PBS containing 50 mM glycine (0.5 mL, 20 min) and the cell plasma membranes were permeabilized with 0.05% Triton X-100 in PBS (0.5 mL, 5 min). The coverslips were soaked in PBS containing 10% (w/v) BSA for 1h, washed with 0.2% acetylated BSA (BSA-c) in PBS (2 x 0.5 mL, 5 min) and then incubated with 6 nM (Nb-E3)₂:(K3)₂AuNP in 0.2% BSA-c containing 10% FCS, 0.5 mL for 1 h. Next the cells were washed with 0.2% BSA-c (2 x 0.5 mL, 5 min) and with 80 mM citrate buffer pH 6.2 (3 x 0.5 mL, 5 min). Finally the AuNPs were made visible using a silver staining protocol modified from the Danscher method as reported previously.⁴⁸

3.6 Pre-embedding immunolabelling and sample preparation for EM

Cells were fixed with 4% PFA in PBS for 20 min at 20°C. The coverslips were washed with PBS (3 x 0.5 mL, 5 min), PBS containing 50 mM glycine (0.5 mL, 20 min) and the cell plasma membranes were permeabilized with 0.05% Triton X-100 in PBS (0.5 mL, 5 min). The coverslips were soaked in PBS containing 10% (w/v) BSA for 1h, washed with 0.2% BSA-c in PBS (2 x 0.5 mL, 5 min) and then incubated with (Nb-E3)₂:(K3)₂AuNP (12 nM in 0.2% BSA-c containing 10% FCS) overnight at 4°C. The next day the cells were washed with PBS (5 x 0.5 mL, 8 min) and were post-fixed with 1% glutaraldehyde in PBS (15 min). The cells were washed with PBS (3 times), with H₂O (5 times) and the AuNPs were enlarged using R-Gent SE-EM Silver Enhancement Reagent (Aurion, 80 min of development). The specimen was then washed with H₂O (5 times) and post-fixed with 0.5% osmium tetroxide (15 min). The specimen was again washed with H₂O, dehydrated with increasing concentrations of ethanol, treated with propylene oxide and flat embedded in Epon. The resin-embedded sample was sectioned into 60 nm thick slices that were deposited onto copper 200 mesh grids (Electron Microscopy Sciences).

High-angle annular dark-field scanning transmission electron microscopy (HAADF-STEM) and energy dispersive X-ray spectroscopy (EDX): Cellular samples were imaged using a Cs-corrected JEOL JEM-2100F scanning transmission electron microscope operating at 200 kV and equipped with a High Angle Annular Dark Field Detector. EDX analysis was performed on the same instrument equipped with a JEOL Silicon Drift Detector (DrySD60GV, sensor size 60 mm²) with a solid angle of 0.6 srad.

4. Conclusion

During our investigation to precisely functionalize AuNPs with the minimal sized Nb, we discovered that the conjugation approach involving the non-covalent assembly between complementary associating peptide tags appended to the AuNP and the nanobody, respectively, yielded probes that specifically bind to GFP. These probes proved highly effective for the visualization of various GFP-protein fusions inside cells by BFM and high resolution HAADF-STEM, thus pointing out the versatility of these gold-tagged Nbs for labelling applications using two different imaging modalities. The synthesis of the probe is convenient to perform: the synthetic steps can be monitored in a straightforward manner and the building blocks can be separately synthesized and stored in accordance with their stability. Moreover, the linkage of the recombinant nanobody to the AuNP at the latest synthetic step (in here after the required pegylation to protected the AuNP from interacting with encountered proteins) is extremely convenient as it limits possible chemical or structural denaturation of the protein. Even if the current probes are mixtures of species (the number of dimerized E3-Nbs per (K3)₂AuNP oscillates around 2), this approach offers by far more control over stoichiometry and orientation of the

attached E3-Nbs than the nanoparticle functionalization via adsorption or EDC chemistry. This non-covalent conjugation approach is clearly implementable for other nanobodies and therefore unlocks the usefulness of future nanobodies targeting proteins for the individual localization of protein inside the cell by EM and possibly cryo EM at unprecedented high resolution.

Author Contributions

NG, MD, GZ, DS, MB, DI and AMH designed and performed experiments; NG, GZ, PS, SO, OE conceived experiments, analysed the data and revised the manuscript, NG and GZ drafted the manuscript.

Conflicts of interest

There are no conflicts to declare.

Acknowledgements

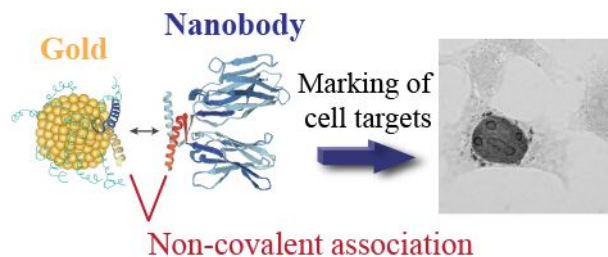
This research was supported by the CNRS 80prime program attributed to GZ, OE and PS, the ITI Innovec (IdEx (ANR-10-IDEX-0002), SFRI (ANR-20-SFRI-0012)) and La Ligue contre le Cancer CCIR-Est). NG was funded by a PhD fellowship from the IdEX Unistra (Université de Strasbourg and Investissement d'Avenir). Transmission electron microscopy observation was performed at Plateforme Imagerie in vitro, CNRS UPS 3156, Strasbourg. We are grateful to Robert Drillien for style-edition of the text.

Notes and references

- 1 L. Schermelleh, A. Ferrand, T. Huser, C. Eggeling, M. Sauer, O. Biehlmaier, Gregor P. C. Drummen, *Nature Cell Biology*, 2019, **21**, 72–84.
- 2 Z. Jiang, X. Jin, Y. Li, S. Liu, X.-M. Liu, Y.-Y. Wang, P. Zhao, X. Cai, Y. Liu, Y. Tang, X. Sun, Y. Liu, Y. Hu, M. Li, G. Cai, X. Qi, S. Chen, L.-L. Du and W. He, *Nature Methods*, 2020, **17**, 937–946.
- 3 W. P. Faulk and G. M. Taylor, *Immunochemistry*, 1971, **8**, 1081–1083.
- 4 E. V. Polishchuk and R. S. Polishchuk, *Tissue and Cell*, 2019, **57**, 103–110.
- 5 R. C. N. Melo, E. Morgan, R. Monahan-Earley, A. M. Dvorak and P. F. Weller, *Nat Protoc*, 2014, **9**, 2382–2394.
- 6 I. Orlov, A. Schertel, G. Zuber, B. Klaholz, R. Drillien, E. Weiss, P. Schultz and D. Spehner, *Scientific reports*, 2015, **5**, 8324.
- 7 M. S. Sirerol-Piquer, A. Cebrián-Silla, C. Alfaro-Cervelló, U. Gomez-Pinedo, M. Soriano-Navarro and J.-M. G. Verdugo, *Micron*, 2012, **43**, 589–599.
- 8 U. Rothbauer, K. Zolghadr, S. Tillib, D. Nowak, L. Schermelleh, A. Gahl, N. Backmann, K. Conrath, S. Muyldermans, M. C. Cardoso and H. Leonhardt, *Nature Methods*, 2006, **3**, 887–889.
- 9 K. Farnaz, B. Mahdi, R. Abbas and K.-L. Fatemeh, *International Reviews of Immunology*, 2018, **37**, 316–322.
- 10 D. Schumacher, J. Helma, A. F. L. Schneider, H. Leonhardt

- and C. P. R. Hackenberger, *Angew. Chem. Int. Ed.*, 2018, **57**, 2314–2333.
- 11 T. Hebbrecht, J. Liu, O. Zwaenepoel, G. Boddin, C. Van Leene, K. Decoene, A. Madder, K. Braeckmans and J. Gettemans, *New Biotechnology*, 2020, **59**, 33–43.
- 12 S. Massa, C. Xavier, J. De Vos, V. Caveliers, T. Lahoutte, S. Muyldermans and N. Devoogdt, *Bioconjug. Chem.*, 2014, **25**, 979–988.
- 13 E. Platonova, C. M. Winterflood, A. Junemann, D. Albrecht, J. Faix and H. Ewers, *Methods*, 2015, **88**, 89–97.
- 14 T. Pleiner, M. Bates, S. Trakhanov, C.-T. Lee, J. E. Schliep, H. Chug, M. Böhning, H. Stark, H. Urlaub and D. Görlich, *Elife*, 2015, **4**, e11349.
- 15 G. Carrington, D. Tomlinson and M. Peckham, *Mol. Biol. Cell*, 2019, **30**, 2737–2740.
- 16 Ben N G Giepmans, *frontiers in Cellular Neuroscience*, 2020, **14**.
- 17 R. D. Brokx, E. Bolewska-Pedyczak and J. Gariépy, *Journal of Biological Chemistry*, 2003, **278**, 2327–2332.
- 18 M. Vigneron, F. Dietsch, L. Bianchetti, A. Dejaegere, Y. Nominé, A. Cordonnier, G. Zuber, B. Chatton and M. Donzeau, *Bioconjug. Chem.*, 2019, **30**, 1734–1744.
- 19 G. M. Clore, J. G. Omichinski, K. Sakaguchi, N. Zambrano, H. Sakamoto, E. Appella and A. M. Gronenborn, *Science*, 1994, **265**, 386–391.
- 20 M. H. Kubala, O. Kovtun, K. Alexandrov and B. M. Collins, *Protein Science*, 2010, **19**, 2389–2401.
- 21 M. Kijanka, E. G. van Donselaar, W. H. Müller, B. Dorresteyn, D. Popov-Čeleketić, M. el Khattabi, C. T. Verrips, P. M. P. van Bergen en Henegouwen and J. A. Post, *Journal of Structural Biology*, 2017, **199**, 1–11.
- 22 N. Ariotti, T. E. Hall, J. Rae, C. Ferguson, K.-A. McMahon, N. Martel, R. E. Webb, R. I. Webb, R. D. Teasdale and R. G. Parton, *Developmental Cell*, 2015, **35**, 513–525.
- 23 N. Ariotti, J. Rae, N. Giles, N. Martel, E. Sierecki, Y. Gambin, T. E. Hall and R. G. Parton, *PLoS Biol.*, 2018, **16**, e2005473.
- 24 J. Goossens, H. Sein, S. Lu, M. Radwanska, S. Muyldermans, Y. G. J. Sterckx and S. Magez, *Anal. Methods*, 2017, **9**, 3430–3440.
- 25 G. Zuber, E. Weiss and M. Chiper, *Nanotechnology*, 2019, **30**, 352001.
- 26 L. Boselli, E. Polo, V. Castagnola and K. A. Dawson, *Angew. Chem.*, 2017, **129**, 4279–4282.
- 27 M. Zhou, C. Zeng, Y. Chen, S. Zhao, M. Y. Sfeir, M. Zhu and R. Jin, *Nature Communications*, 2016, **7**, 1–7.
- 28 C. J. Ackerson, P. D. Jadzinsky, G. J. Jensen and R. D. Kornberg, *Journal of the American Chemical Society*, 2006, **128**, 2635–2640.
- 29 C. J. Ackerson, R. D. Powell and J. F. Hainfeld, in *Methods in Enzymology*, Elsevier, 2010, vol. 481, pp. 195–230.
- 30 C. Leduc, S. Si, J. Gautier, M. Soto-Ribeiro, B. Wehrle-Haller, A. Gautreau, G. Giannone, L. Cognet and B. Lounis, *Nano Lett.*, 2013, **13**, 1489–1494.
- 31 D. Desplancq, N. Groysbeck, M. Chiper, E. Weiss, B. Frisch, J.-M. Strub, S. Cianferani, S. Zafeiratos, E. Moeglin, X. Holy, A. L. Favier, S. De Carlo, P. Schultz, D. Spohner and G. Zuber, *ACS Applied Nano Materials*, 2018, **1**, 4236–4246.
- 32 N. Groysbeck, A. Stoessel, M. Donzeau, E. C. da Silva, M. Lehmann, J.-M. Strub, S. Cianferani, K. Dembélé and G. Zuber, *Nanotechnology*, 2019, **30**, 184005.
- 33 A. Stoessel, N. Groysbeck, L. Guyot, L. Barret, Y. Nominé, L. Nguekeu-Zebaze, A. Bender, L. Voilquin, T. Lutz, N. Pallaoro, M. Blocat, C. Deville, M. Masson, G. Zuber, B. Chatton and M. Donzeau, *Bioconjug. Chem.*, 2020, **31**, 2421–2430.
- 34 R. Lévy, N. T. K. Thanh, R. C. Doty, I. Hussain, R. J. Nichols, D. J. Schiffrin, M. Brust and D. G. Fernig, *Journal of the American Chemical Society*, 2004, **126**, 10076–10084.
- 35 G. Zuber, L. Zammuto-Italiano, E. Dauty and J.-P. Behr, *Angew. Chem. Int. Ed. Engl.*, 2003, **42**, 2666–2669.
- 36 M. Chiper, N. Tounsi, R. Kole, A. Kichler and G. Zuber, *J Control Release*, 2017, **246**, 60–70.
- 37 G. Vauquelin and S. J. Charlton, *British Journal of Pharmacology*, 2013, **168**, 1771–1785.
- 38 H. D. Herce, M. Rajan, G. Lättig-Tünnemann, M. Fillies and M. C. Cardoso, *Nucleus*, 2014, **5**, 590–600.
- 39 B. M. Humbel, M. D. de Jong, W. H. Müller and A. J. Verkleij, *Microsc. Res. Tech.*, 1998, **42**, 43–58.
- 40 H. Kimura and P. R. Cook, *J. Cell Biol.*, 2001, **153**, 1341–1353.
- 41 T. Kanda, K. F. Sullivan and G. M. Wahl, *Curr. Biol.*, 1998, **8**, 377–385.
- 42 W. K. M. Lai and B. F. Pugh, *Nat Rev Mol Cell Biol*, 2017, **18**, 548–562.
- 43 U. Schnell, F. Dijk, K. A. Sjollem and B. N. G. Giepmans, *Nature Methods*, 2012, **9**, 152–158.
- 44 G. Freund, D. Desplancq, A. Stoessel, R. Weinsanto, A.-P. Sibling, G. Robin, P. Martineau, P. Didier, J. Wagner and E. Weiss, *J. Mol. Recognit.*, 2014, **27**, 549–558.
- 45 X. Liu, M. Atwater, J. Wang and Q. Huo, *Colloids and Surfaces B: Biointerfaces*, 2007, **58**, 3–7.
- 46 C. Chandrashekhar, B. Pons, C. D. Muller, N. Tounsi, R. Mulherkar and G. Zuber, *Acta Biomater.*, 2013, **9**, 4985–4993.
- 47 J. B. Gossart, E. Pascal, F. Meyer, E. Heuillard, M. Gonçalves, F. Gossé, E. Robinet, B. Frisch, C. Seguin and G. Zuber, *Global Challenges*, 2017, **1**, 1700013.
- 48 R. W. Burry, D. D. Vandredre and D. M. Hayes, *J. Histochem. Cytochem.*, 1992, **40**, 1849–1856.

Nanobodies and thiolate-coated gold nanoparticles of circa 2 nm diameters are attractive elements for building multifunctional assemblies. A specific and non-covalent approach is reported to associate the targeting ability of nanobodies with the detectability of 2.4 nm gold nanoparticles for immunolabelling of cellular effectors using light and high-resolution electron microscopy.



Supporting Information

Gold Labelling of Green Fluorescent Protein (GFP)-tag inside cells using recombinant nanobodies conjugated to 2.4 nm thiolate-coated gold nanoparticles

*Nadja Groysbeck, Mariel Donzeau, Audrey Stoessel, Anne-Marie Haeberle, Stéphane Ory, Danièle Spehner, Patrick Schultz, Ovidiu Ersen, Mounib Bahri, Dris Ihiawakrim, Guy Zuber**

Table of content

Materials and Methods (Addition to the main article)

Figure S1. DNA and amino acid sequences of GFP nanobody constructs and analysis of the construct stability as reported	S-7
Figure S2. Evaluation of the apparent binding affinities of GFP nanobody and mutated Nb-C7 for adsorbed GFP using ELISA.	S-8
Figure S3. Direct conjugation of nanobody to thiolate-coated AuNPs.	S-9
Figure S4. Analysis of Integrity of Nb- construct	
Figure S5. Reaction products after addition of the thiolated E3 to AuG gold	S-10
Figure S6. Gold labeling of H2B-GFP HeLa using un-pegylated Nb-AuNP conjugate.	S-11
Figure S7 Statistical analysis of (Nb-E3) ₂ :(K3) ₂ AuNP size distribution and clustering	S12
Figure S8. Fluorescent and (Nb-E3) ₂ :(K3) ₂ AuNP-mediated detection of protein-GFP fusions after transient gene transfection.	S13
Figure S9. Comparison of immunodetection ability of (Nb-E3) ₂ :(K3) ₂ AuNP into GFP-PCNA-interacting peptide (PIP) HeLa cells after fixation with 4%PFA or 2% PFA containing 0.02% glutaraldehyde	S14
Figure S10. Comparison of immunodetection ability of (Nb-E3) ₂ :(K3) ₂ AuNP in H2B-GFP HeLa cells fixed with 4% PFA or 2% PFA containing 0.02%glutaraldehyde.	S15
Figure S11. Preparation and analysis of the IgG-AuNP conjugate.	S16
Figure S12. Fluorescent and silver-enhanced images of H2B-GFP HeLa cells after IgG and IgG-AuNP -mediated detection of GFP.	S17

Figure S13. Fluorescent images of H2B-GFP HeLa cells after IgG-mediated detection of GFP. S18

Figure S14. Fluorescent images of H2B-GFP HeLa cells after IgG-mediated detection of GFP. S19

Figure S15. Analysis of $(\text{Nb-E3})_2:(\text{K3})_2\text{AuNP}$ ability to detect GFP into H2B-GFP HeLa cells several days after assembly and evaluation of the sequential immunogold labelling methodology. S20

Figure S16. EDX spectroscopy analysis of a nuclear portion of H2B-GFP HeLa after gold immunolabeling with $(\text{Nb-E3})_2:(\text{K3})_2\text{AuNP}$ without silver-enhancement. S21

Figure S17. EDX spectroscopy analysis of nuclear portion of the H2B-GFP HeLa specimen after gold immunolabeling with $(\text{Nb-E3})_2:(\text{K3})_2\text{AuNPs}$ and silver enhancement. S22

Figure S18. Pre-embedding immuno-EM of the histone protein H2B-GFP with $(\text{Nb-E3})_2:(\text{K3})_2\text{AuNP}$. S23

Materials and Methods (Addition to the main article)

Materials: The AuG was synthesized as previously reported with a diameter of 2.4 nm.¹ The peptides were ordered from GeneCust in purity above 80%. The 2000 Da alpha-methoxy-omega-mercapto poly(ethylene glycol) (PEG) was ordered from Iris Biotech. Electron microscopy grade paraformaldehyde (20% w/v solution) and glutaraldehyde (25% w/v solution) were purchased from Electron Microscopy Sciences. Other reagents were obtained from Sigma Aldrich, Carl Roth, VWR Chemicals, Euromedex or Honeywell. They were used without further purification unless stated otherwise. All solutions and buffers were made with water purified with a Millipore Q-POD apparatus. Precision Plus Protein Standard Dual Xtra (BioRad) was used as protein ladder for SDS-PAGE analysis. The affinity-purified goat IgG directed against the nanobody domain was purchased from Jackson ImmunoResearch. The donkey anti-goat IgG (H+L) antibody conjugated to Alexa Fluor Plus 594 was purchased from Invitrogen. BSA-c was bought as 10% solution from Aurion. DNA transfection was performed with the *in vitro* transfection reagent jetOPTIMUS from Polyplus-transfection. Ni NTA agarose beads were purchased from Qiagen.

Specific equipment: A HI 2210 pH meter was used for measuring the pH of buffer solutions. Centrifugation of 50 mL tubes was done using an Eppendorf 5810R centrifuge equipped with an A-4-81 rotor. For smaller volumes (0.1 – 2 mL) centrifugation was performed in an Eppendorf 5415R centrifuge. AuNP reaction solutions were shaken on a Heidolph Rotamax 120 rocking platform. Functionalized AuNPs were concentrated and purified using Amicon Ultra 0.5 mL centrifugal devices (MWCO 30 kDa, if not stated otherwise).

Determination of AuNP concentration: Concentrations of AuNPs were determined spectrophotometrically by measuring the absorbance at 520 nm. The extinction coefficient of the AuNP was determined using the formula $\ln(\epsilon) = k \cdot \ln(D) + a$ reported by Liu *et al.*² ϵ = extinction coefficient ($M^{-1} \text{ cm}^{-1}$), D = AuNP core diameter in nm, $k= 3.32111$, $a = 10.80505$. From the measured diameter of 2.4 nm, the formula yields an $\epsilon_{520 \text{ nm}}$ of $89\,6771 \text{ M}^{-1} \text{ cm}^{-1}$ for AuG.

Denaturing and native polyacrylamide gel electrophoresis (PAGE) analyses: Denaturing sodium dodecylsulfate (SDS)-PAGE analysis was performed following a published protocol from Laemmli *et al.* on 15% or 5 – 18% polyacrylamide gradient gels. A 20 min pre-run at 20 mA was performed prior to loading the samples onto the gel. The AuNP samples were loaded onto the gel by dilution with 50% (v/v) glycerol to a final glycerol concentration of 5% (v/v). AuNPs were visible on the gels as black-brown bands. Proteins were revealed in blue by Coomassie blue staining. Titration of the non-covalent assemblies between (Nb-E3)₂ and (K3)₂AuNP before and after pegylation was performed by PAGE analysis in the absence of SDS.

Enzyme Linked Immunosorbent Assay (ELISA): The ELISA plates were prepared as follows: GFP (1 $\mu\text{g}/\text{mL}$ in PBS) was adsorbed onto wells of immunosorbent plates (Thermo Scientific) by an overnight incubation at 4°C. The remaining adsorbing surfaces were then blocked with 3% BSA in PBS (200 μL per well) for 1 h. Binding of AuNP-nanobody conjugates to plastic-adsorbed GFPs was then evaluated by incubating various concentrations of the conjugates (1 h, 100 μL per well). The bound conjugates were then detected with sequential incubation with a goat anti-V_HH Alpaca IgG (2.5 $\mu\text{g}/\text{mL}$, 1h), an anti-goat-HRP antibody (1:1000 dilution, 100 μL per well, 1 h) and then tetramethylbenzidine (TMB) (100 μL of a 10 mg/mL solution in 0.1 M sodium acetate, pH 6) in the presence of 0.007% hydrogen peroxide. Between incubations, the wells were washed three times with PBS containing 0.1% NP40 and three

times with PBS. Transformation of TMB in a colored product was stopped with 1 M sulfuric acid (50 μ L per well) and the color signal was measured with an ELISA plate reader (BioRad 550) at 450 nm. The binding of the AuNP-nanobody conjugates was alternatively evaluated by detection of the AuNP moiety. The binding of AuNP-nanobody conjugates to GFP-adsorbed surface was performed as described above. The AuNPs were then amplified in the dark for 15 min using a published silver developing solution.³

Cell Culture: Cells were cultured in a 37°C humidified incubator supplied with 5% CO₂. HeLa and stably transformed H2B-GFP HeLa cells were maintained in Dulbecco's modified Eagle medium containing 2 mM L-glutamine, 10 mM HEPES buffer, pH 7.0, 10% heat-inactivated fetal bovine serum (FBS) and 50 μ g/mL gentamycin. For immunocytochemistry, immunofluorescence and pre-embedding immuno-EM experiments, cells (25000 cells/well) were seeded into 24-well plates in 0.5 mL cell culture medium and were let to adhere on glass coverslips overnight.

Genetic engineering of the point mutation GFP nanobody variants : The GFP nanobody (Nb)⁴ was engineered to contain either a Serine 7 to Cysteine point mutation (C7-Nb), a Cterminal cysteine (C143-Nb) (Supporting information, Figure S1). Thiolated variants were constructed from the GFP nanobody gene using the PCR methodology and the following primers: 5'-GGAGAT ATACCA TGGGGT CCCAGG TTCAGC TGGTTG AATGTG GTGGTG-3' and 5'CACTAG TTGCGG CCGCTG AGGAGA CGGT-3'. The amplified DNA fragment was then digested with *NcoI* and *NotI* restriction enzymes and inserted into a pETOM vector encoding a c-myc sequence and a his6 tag.⁵

Expression and purification of anti-GFP nanobody variants: Recombinant his-tagged C7-Nb and C143-Nb were expressed in *E. coli* BL21(DE3)pLys after induction with 1 mM IPTG in 100 mL LB medium at 20°C for 24h. The bacteria were lysed by ultrasonication and the his-tagged proteins were purified by immobilized metal affinity chromatography using a HisTrap

HP column (1 mL) charged with NiSO₄ and then by gel filtration on a HiLoad Superdex 200 pg preparative column operating at a flow rate of 0.5 mL/min. Protein fractions were analyzed by SDS-PAGE. Selected fractions were pooled and protein solutions were concentrated with Amicon Ultra 4 mL centrifugal devices (MWCO 3 kDa).

Direct Au-S conjugation approach: A 40 μM solution of C7-Nb (75 μL, 3 nmol) was incubated with 0.4 mM TCEP (25 μL, 10 nmol) for 15 minutes at 25°C in 0.1 M HEPES, pH 7.5 to reduce disulfides to thiols. A portion of this mixture (88 μL of a 30 μM solution, 2.64 nmol) was then mixed with a 42 μM solution of the AuNP (250 μL, 10.5 nmol) to obtain a molecular AuNP/Nb ratio of 4. After an overnight incubation at 25°C, the alpha-methoxy-omega-mercapto poly(ethylene glycol) (818 μL of a 1 mM aqueous solution, 818 nmol) was added and the passivation reaction was allowed to proceed at 25°C for 2h. The released ligands and unreacted thiolated molecules were then separated from the AuNPs by ultrafiltration methodology using Amicon 30 K ultracentrifugal devices (5 washes with PBS). The fraction containing the AuNPs was further purified using Ni-NTA agarose beads (100 μL beads, equilibrated in PBS) by mixing the crude reaction mixture with the beads under mild agitation for 1.5 h in PBS. The beads were washed three times with PBS (1 mL), two times with 15 mM imidazole in PBS (1 mL) and the AuNP-nanobody conjugate was eluted with 500 μL of PBS containing 200 mM imidazole. The eluate was concentrated to a volume of 100 μL.

Transmission electron microscopy (Figure S6): Cellular specimens were imaged on a Hitachi H7500 transmission electron microscope (Hitachi High Technologies Corporation) equipped with an AMT Hamatsu digital camera (Hamatsu Photonics).

A. GFP Nanobody C7 mutant: DNA sequence

ATGCAGGTTCAACTGGTGGAAAGCGGCGGTGCTCTGGTACAACCGGGCGGTAGTCTGCGCCTG
 AGCTGTGCCGCAAGCGGTTTTCCAGTCAACCGCTACTCTATGCGTTGGTATCGCCAGGCGCCTG
 GTAAAGAACGTGAATGGGTTGCCGGCATGAGCAGTGC GGGCGATCGTTCTAGTTACGAGGACTC
 TGTTAAAGGTCGTTTTACAATTAGCCGTGATGATGCGCGCAATACCGTGTATCTGCAAATGAACA
 GTCTGAAGCCGGAGGACACCGCAGTATATTATTGCAATGTCAACGTGGGGTTTTGAATATTGGGGC
 CAGGGGACTCAGGTGACGGTGAGCTCTAAACATCACCATCACCATCAC

Amino acid sequence of the GFP Nanobody Nb-C7

mQVQLVE^SCGGALVQPGGSLRLSCAASGFPVNRYSMRWYRQAPGKEREWVAGMSSAGDRSSYEDS
 VKGRFTISRDDARNTVYLQMNSLKPEDTAVYYCNVNVGFYWGQGTQVTVSSKHHHHHH

B. GFP Nanobody-C143: DNA sequence

ATGGGGTCCCAGGTTCACTGGTTGAAAGTGGTGGTGCCTGGTACAACCGGGCGGTAG
 TCTGCGCCTGAGCTGTGCCGCAAGCGGTTTTCCAGTCAACCGCTACTCTATGCGTTGGTA
 TCGCCAGGCGCCTGGTAAAGAACGTGAATGGGTTGCCGGCATGAGCAGTGC GGGCGATC
 GTTCTAGTTACGAGGACTCTGTTAAAGGTCGTTTTACAATTAGCCGTGATGATGCGCGCAAT
 ACCGTGTATCTGCAAATGAACAGTCTGAAGCCGGAGGACACCGCAGTATATTATTGCAATGT
 CAACGTGGGGTTTTGAATATTGGGGCCAGGGGACCCAGGTCACCGTCTCCTCAGCGGCCG
 CAACTAGTGAACAAAACATCTCAGAAGAGGATCTGCGCGCTAGCGCACATCACCATCA
 TCACCATTGT

Amino acid sequence of the GFP Nanobody Nb-C143

mGSQVQLVESGGALVQPGGSLRLSCAASGFPVNRYSMRWYRQAPGKEREWVAGMSSAGDR
 SSYEDSVKGRFTISRDDARNTVYLQMNSLKPEDTAVYYCNVNVGFYWGQGTQVTVSSAAAT
 SEQKLISEEDLRASAHHHHHHH**C143**

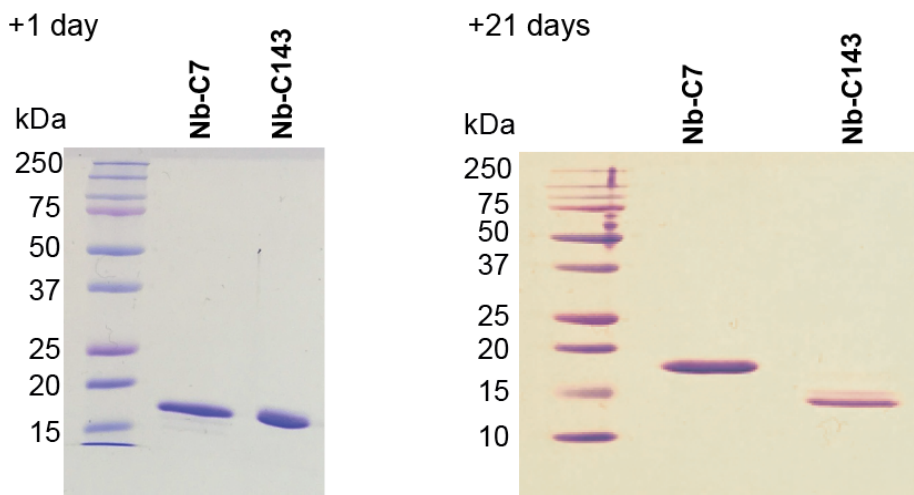
C. Analysis of the stability at 4°C of purified Nb-C7 and Nb-C143 21 days after purification showed fast degradation of the Nb-C143

Figure S1. A and B. DNA and amino acid sequences of GFP nanobody constructs. C. Analysis of the construct stability as reported.

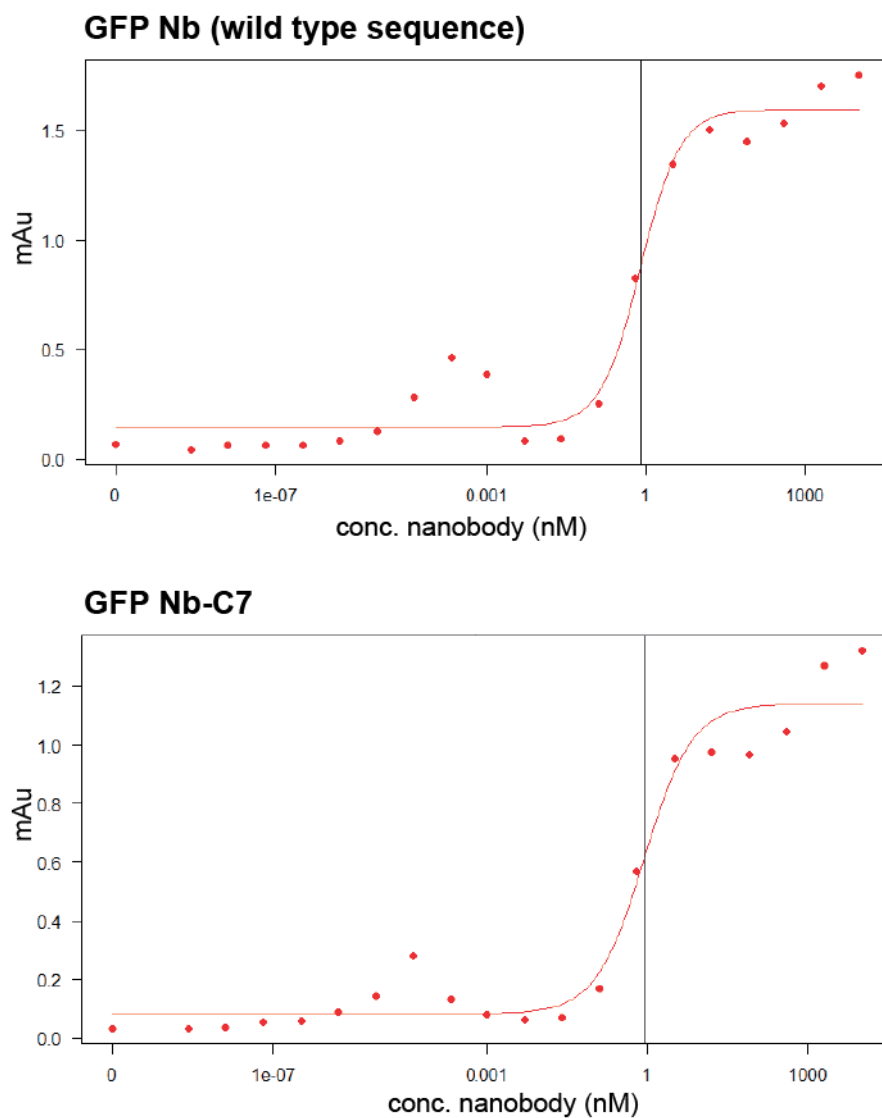


Figure S2. Evaluation of the apparent binding affinities of GFP nanobody and mutated Nb-C7 for adsorbed GFP using ELISA. Data revealed apparent K_d s of 0.78 and 0.87 nM for the wt Nb and Nb-C7 respectively, suggesting that the point mutation did not alter the apparent affinity of the nanobody for GFP.

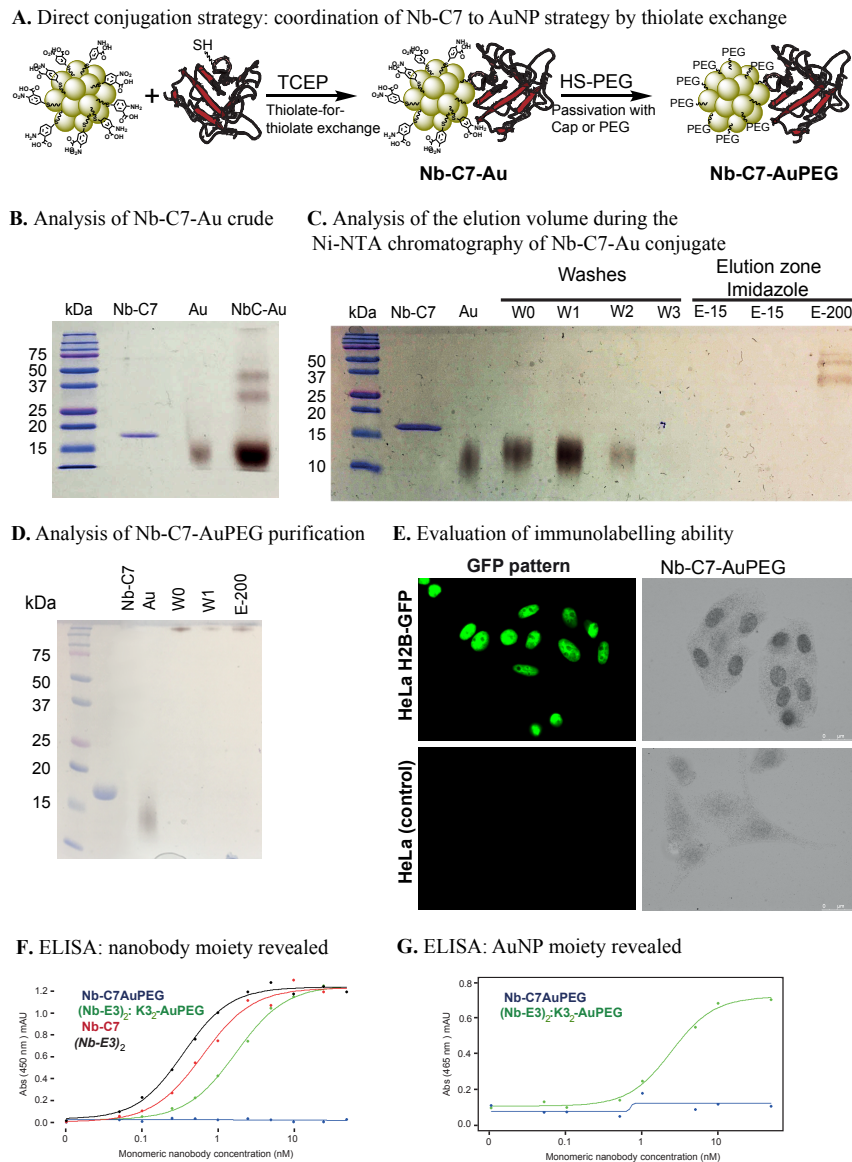


Figure S3. A. Illustration of the direct conjugation of nanobody to thiolate-coated AuNPs. The point mutated C7 nanobody (Nb-C7) was added to TNB/TAB-coated AuNP to obtain the Nb-C-Au by thiolate exchange. TNB/TAB ligands were further exchanged with thiolated PEG for passivation. B. SDS-PAGE of crude products (Nb-C-Au) of reaction between the AuNP (Au) and the thiolated nanobody (Nb-C7) as indicated. B. SDS-PAGE showing affinity purification of unpegylated Nb-C-Au using Ni NTA agarose beads. W0-W3 = wash fractions (PBS), E-15 mM: PBS fractions containing 15 mM imidazole. E-200: PBS with 200 mM imidazole, yielding NbCAu. D. Analysis of the eluted fractions from the Ni-NTA chromatography for purification of NbC-AuPEG. E. Fixed and permeabilized cells were incubated with NbC-AuPEG and then washed to remove unbound probes. The conjugates were revealed by silver staining. F and G. Evaluation of the binding ability of the probes for adsorbed GFP. The bound probes were detected using either anti-Nb antibody (F) or silver (G). Data demonstrate that the Nb-C-AuPEG does not bind to GFP.

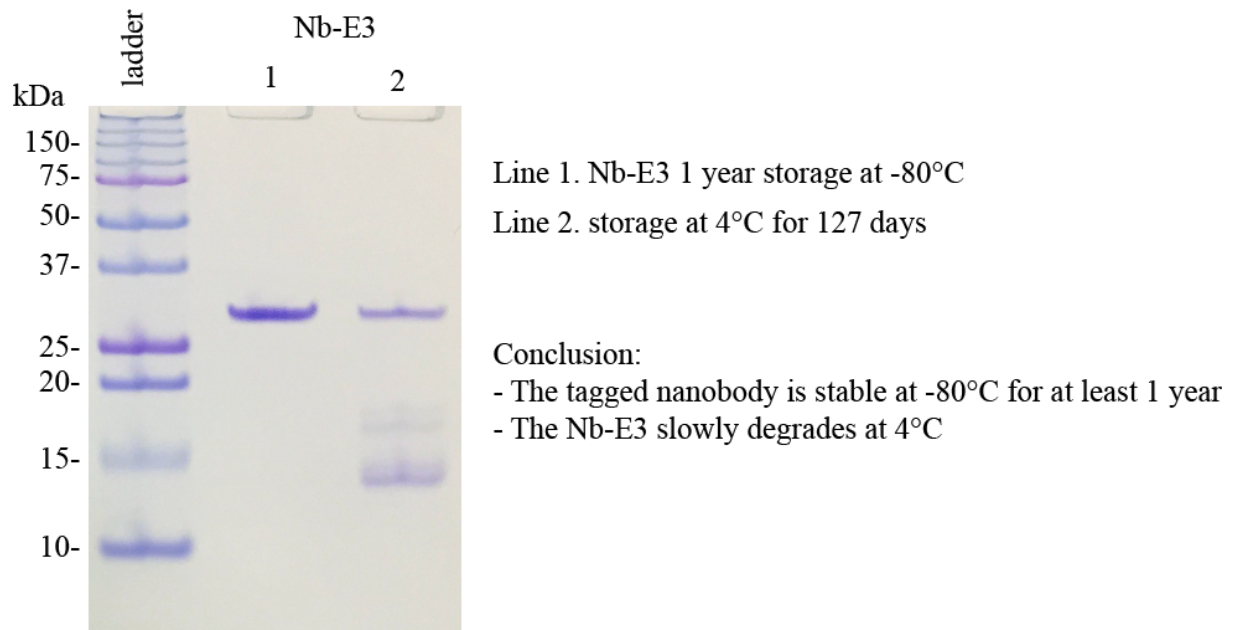


Figure S4. PAGE Analysis of the Nb-E3 construct integrity after storage at -80°C for > 1 year (line 1) and storage at 4°C for 127 days (line 2).

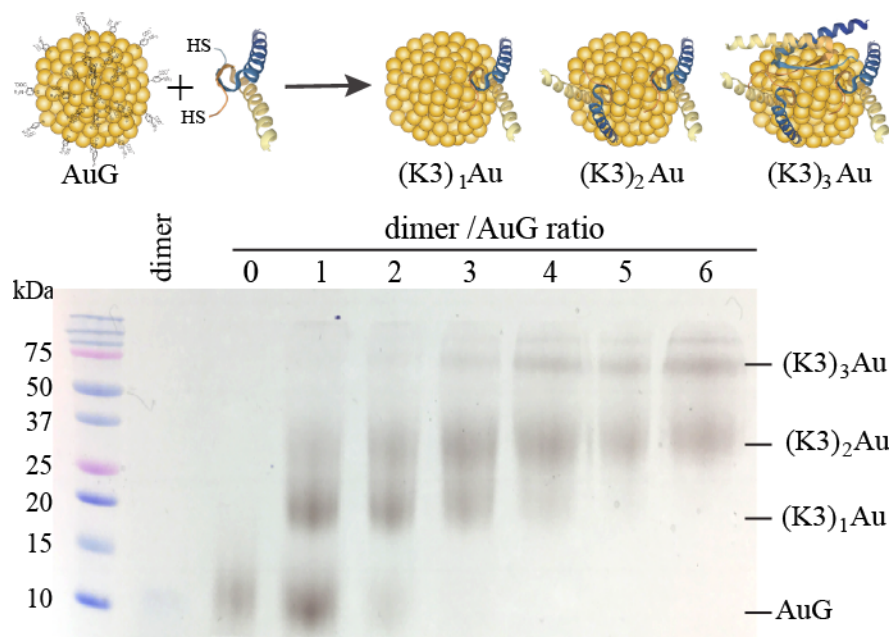
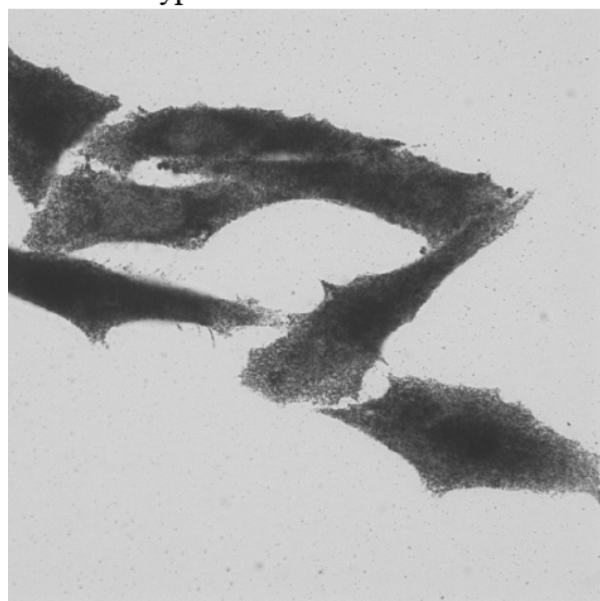


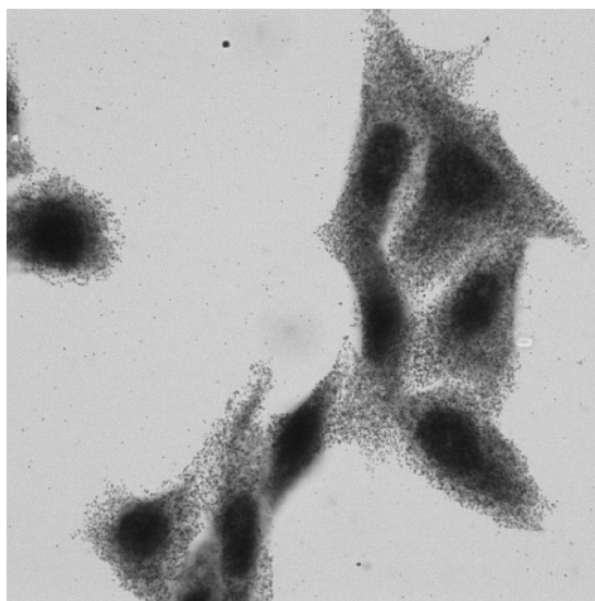
Figure S5. Synthetic scheme and PAGE analysis of the reaction products after addition of the thiolated peptide dimer to AuG gold nanoparticle in water at the indicated dimer/AuG molar ratio.

A. GFP labeling of fixed cells using $(\text{Nb-E3})_2:(\text{K3})_2\text{Au}$ (unpegylated)

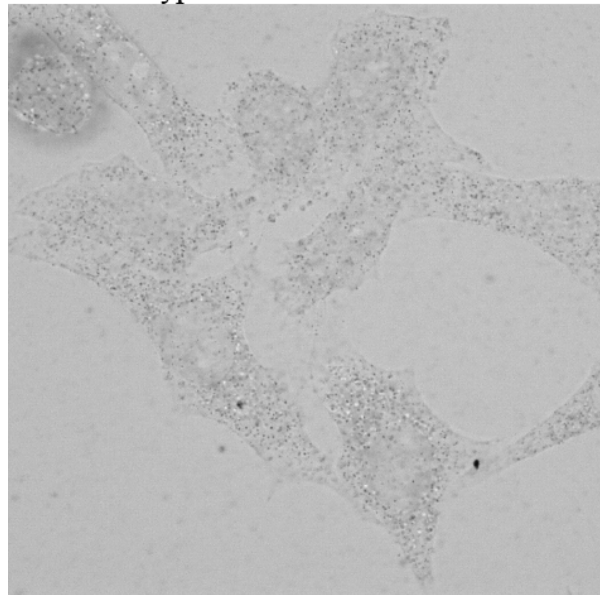
HeLa wild type - control-



H2B-GFP HeLa

**B. GFP labeling of fixed cells using pegylated $(\text{Nb-E3})_2:(\text{K3})_2\text{Au}$**

HeLa wild type - control-



H2B-GFP HeLa

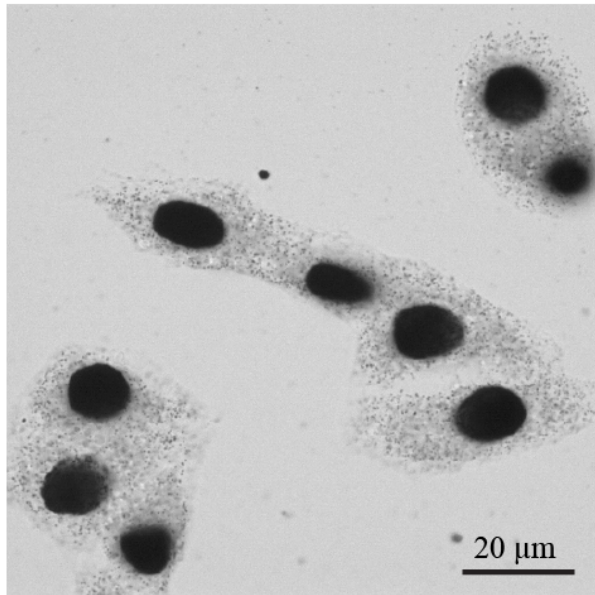
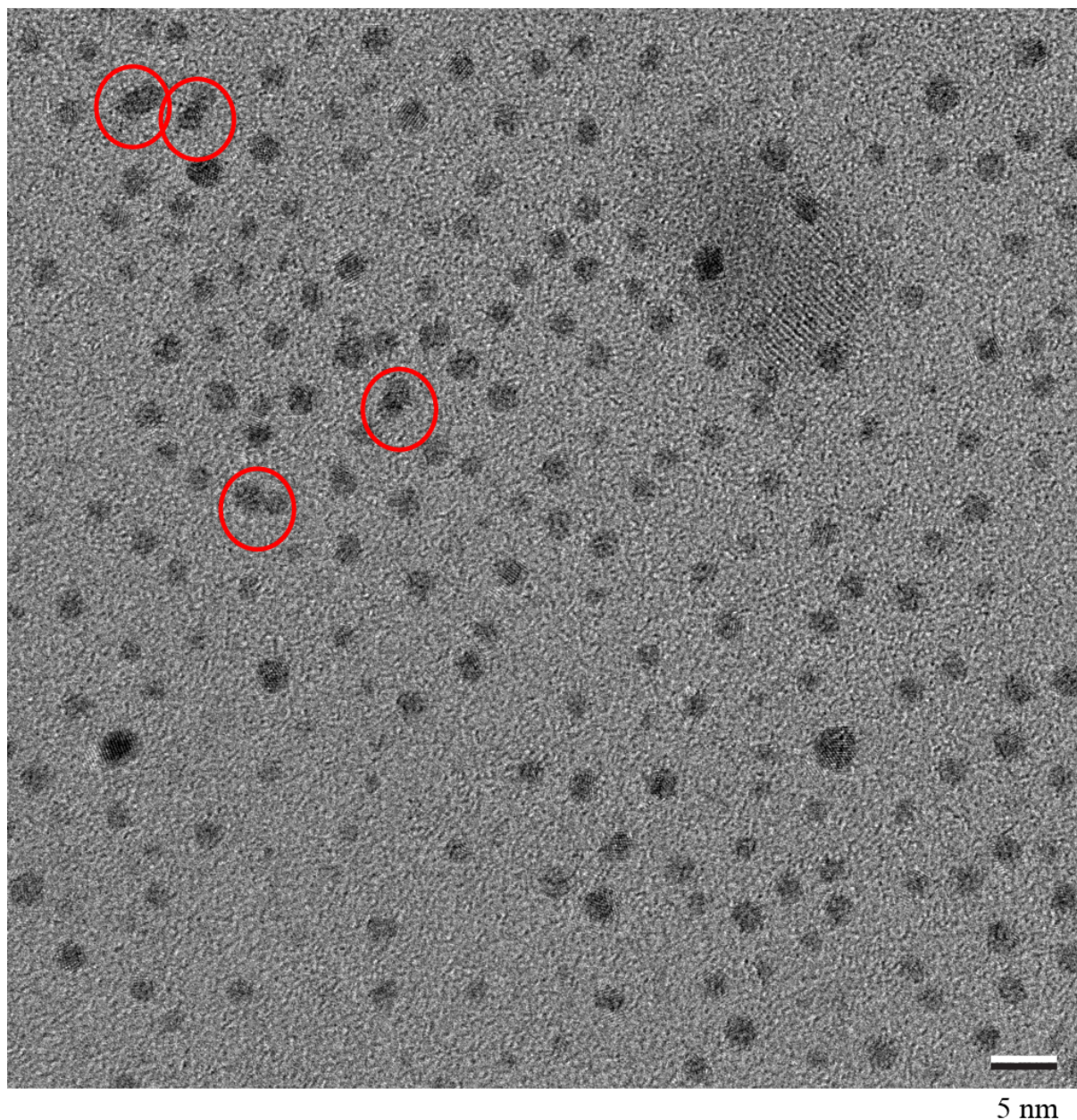


Figure S6. Light microscopy images of GFP labeling of fixed cells HeLa and H2B-GFP HeLa using unpegylated and the pegylated $(\text{Nb-E3})_2:(\text{K3})_2\text{AuNP}$ probes as indicated. The cell membrane was permeabilized. The cells were then incubated with 6 nM of the $(\text{Nb-E3})_2:(\text{K3})_2\text{AuNP}$ conjugates, washed, and the gold nanoparticles bound to cellular components were detected by extensive silver enhancement.

TEM image of $(\text{Nb-E3})_2:(\text{K3})_2 \text{AuNP}$ **Statistical analysis:**

Number of counted particles: 180

Mean diameter: 2.31 nm

Median diameter: 2.38 nm

Standard deviation: 0.35 nm

Dual particles: 4 (2.2%) as indicated by circle

Figure S7. Image used for measuring the size of the gold nanoparticle of $(\text{Nb-E3})_2:(\text{K3})_2 \text{AuNPs}$ and the eventual clustering. Out of the 180 particles present in the field, 4 couples as marked by the red circle were observed.

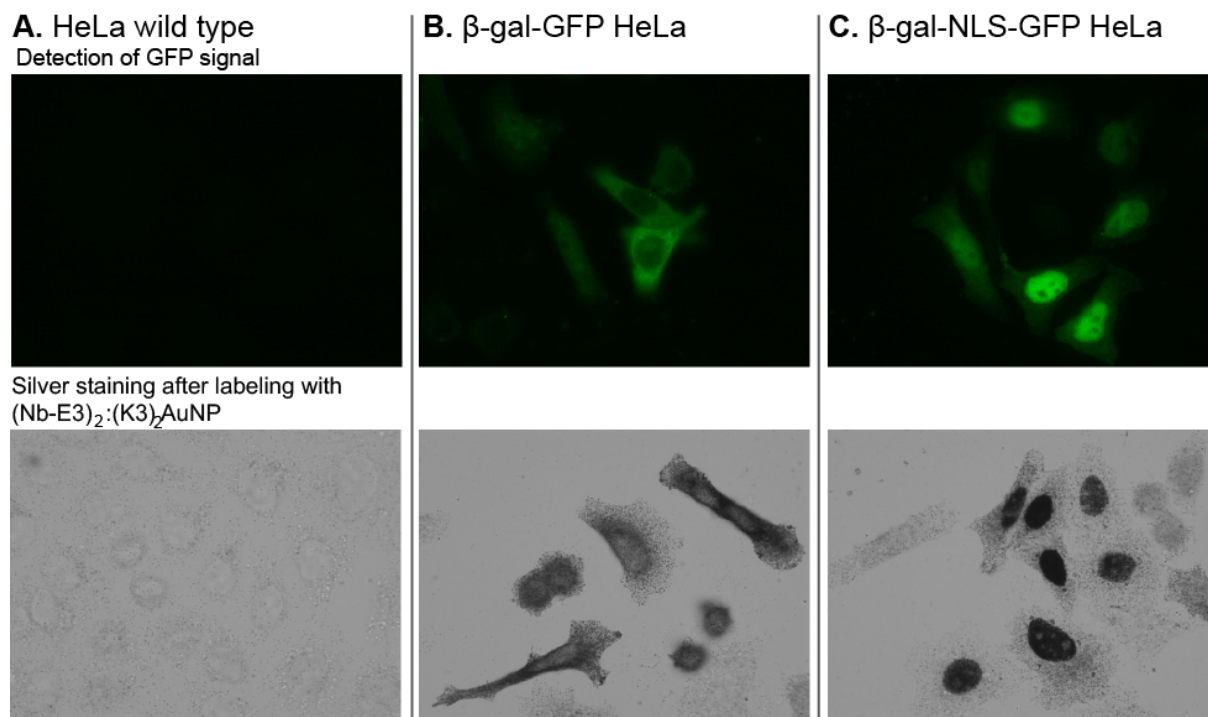


Figure S8. Fluorescent and $(\text{Nb-E3})_2:(\text{K3})_2\text{AuNP}$ -mediated detection of protein-GFP fusions after transient gene transfection. HeLa cells were transiently transfected with DNA plasmids to express β -Galactosidase-GFP (β -Gal-GFP) or β -Galactosidase-Nuclear Localization Signal-GFP (β -Gal-NLS-GFP). Upper images: Detection of the GFP signal in PFA-fixed HeLa cells 24 after DNA plasmid transfection. Lower images: The cell membrane was further permeabilized. The cells were incubated with 6 nM $(\text{Nb-E3})_2:(\text{K3})_2\text{AuNP}$, washed and the gold nanoparticles bound to cellular components were detected by extensive silver enhancement.

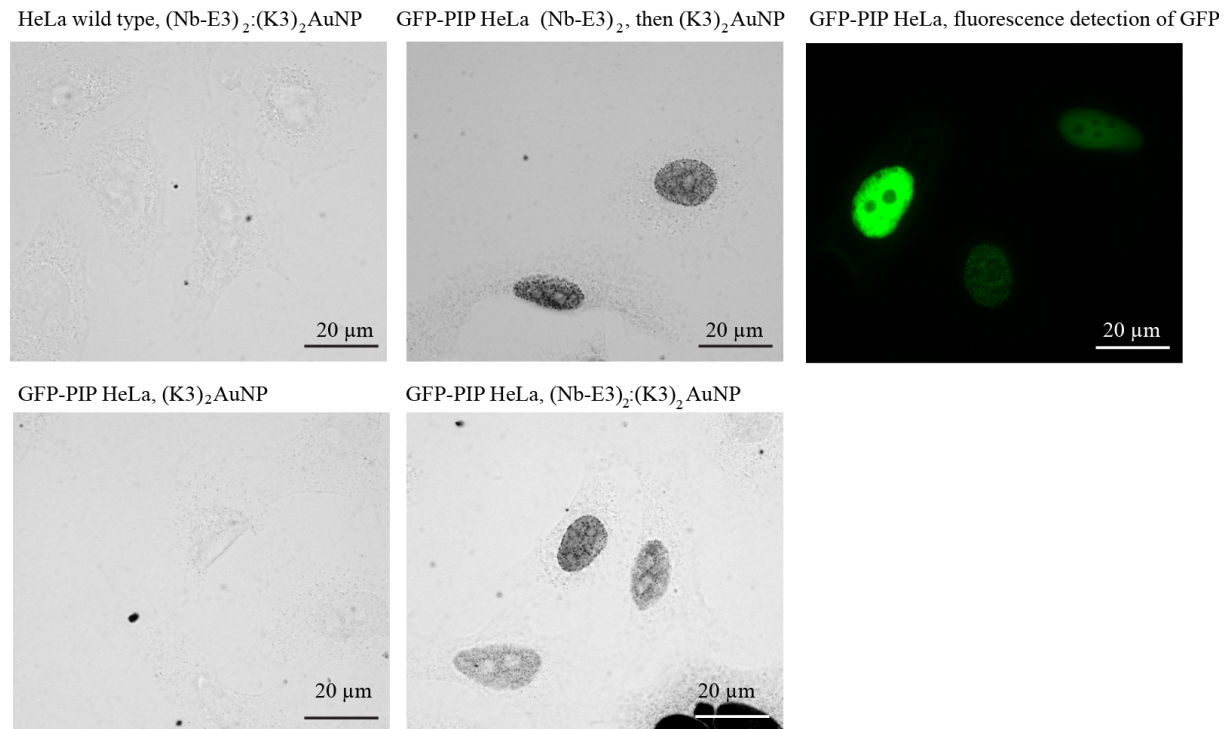
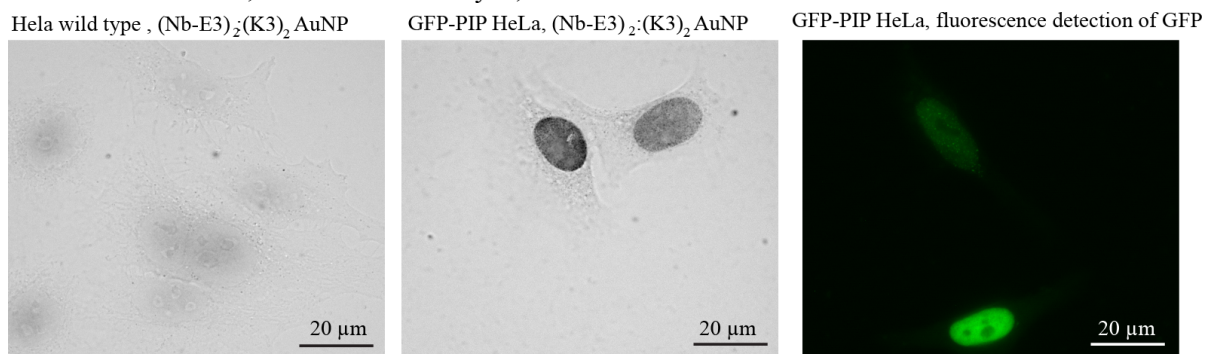
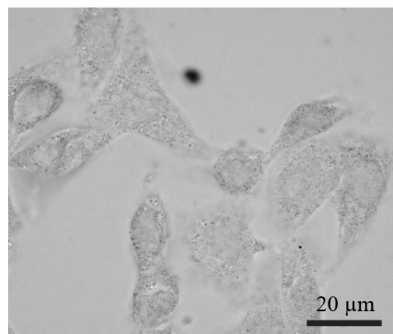
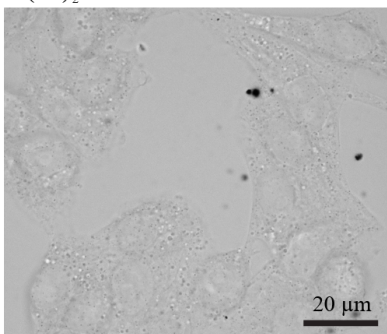
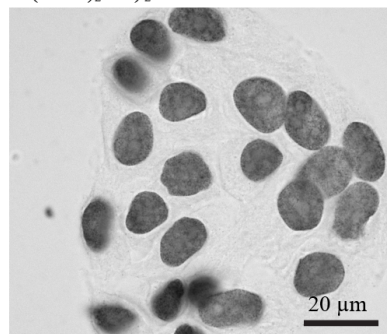
A. Fixation: 4% PFA, Permeabilization: 0.1% Triton X-100**B. Fixation: 2% PFA, 0.02% Glutaraldehyde, Permeabilization: 0.1% Triton X-100**

Figure S9. Comparison of immunodetection ability of (Nb-E3)₂:(K3)₂AuNP into GFP-PCNA-interacting peptide (PIP) HeLa cells after fixation with 4%PFA or 2% PFA containing 0.02% glutaraldehyde.⁶ The GFP-PIP expressing HeLa cells were obtained by transfection of HeLa cells with a modified PEI⁷ and the plasmid fusion (pβA-eGFP-con1-NLS) encoding the GFP-PIP under the control of the β-actin promoter.⁵ 24h after transfection, the cells were fixed for 30 min in 0.2M HEPES, PH 7.4, containing either 4% PFA or 2% PFA, 0.02% glutaraldehyde. The cells were then permeabilized with 0.1% Triton X-100 in PBS. The HeLa cells were then incubated with: - (K3)₂AuNP, ; - (Nb-E3)₂, 3 washing steps (3 times 0.3% BSAC in PBS) and (K3)₂AuNP; - (Nb-E3)₂:(K3)₂AuNP (16 nM). Solution of incubation was PBS containing 10% FBS. After the washing steps, the specimen-bound gold particles cells were detected after silver enhancement. Fluorescent images showed that 80% of the cells were expressing nuclear PIP-GFP at various levels.

A. Fixation: 4% PFA, Permeabilization: 0.1% Triton X-100

1. Cell alone

2. (K3)₂AuNP3. (Nb-E)₂:(K3)₂AuNP**B. Fixation: 2% PFA, 0.02% Glutaraldehyde, Permeabilization: 0.1% Triton X-100**

1. Cell alone

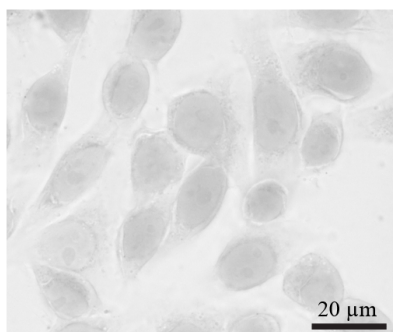
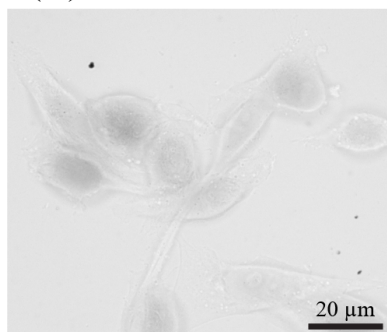
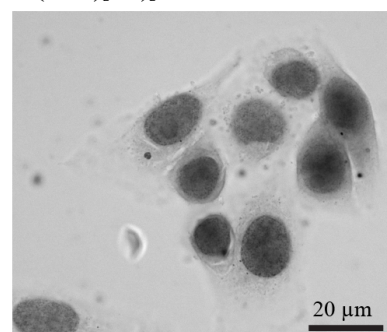
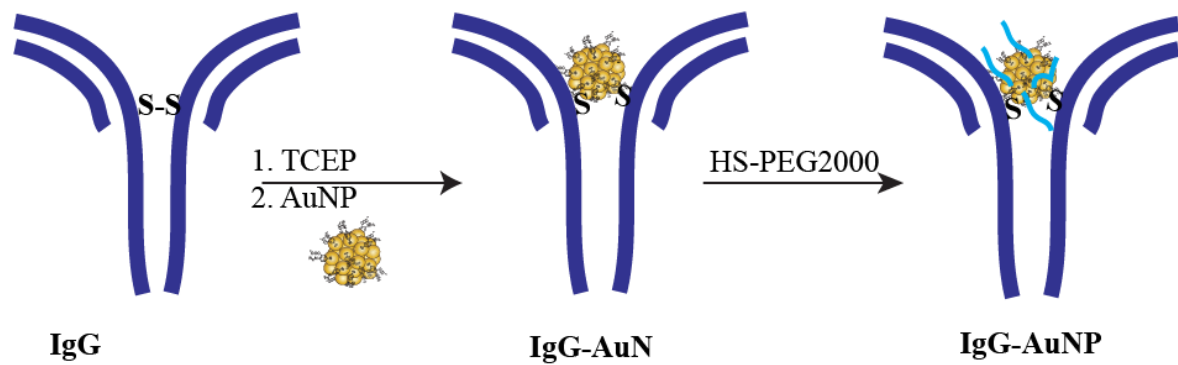
2. (K3)₂AuNP3. (Nb-E)₂:(K3)₂AuNP

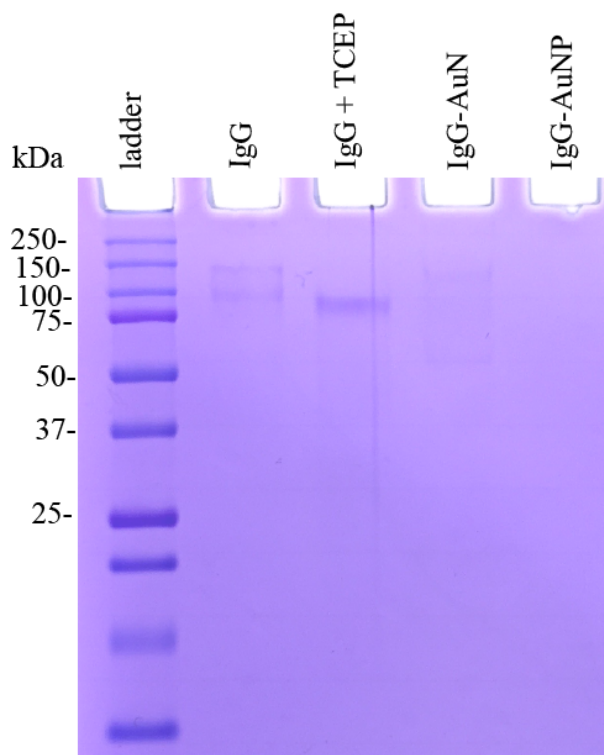
Figure S10. Comparison of immunodetection ability of (Nb-E3)₂:(K3)₂AuNP in H2B-GFP HeLa cells fixed with 4% PFA or 2% PFA containing 0.02% glutaraldehyde.⁶ The H2B-GFP cells were fixed for 30 min in 0.2M HEPES, PH 7.4, containing either 4% PFA or 2% PFA, 0.02% glutaraldehyde. After fixation, the cells were permeabilized with 0.1% Triton X-100 in PBS (20min). The H2B-GFP HeLa cells were then incubated with (K3)₂AuNP and (Nb-E3)₂:(K3)₂AuNP (16 nM) in PBS containing 10% FBS. After the washing steps, the specimen-bound gold particles cells were detected by silver enhancement.

A. Scheme for conjugation and passivation of AuNP to a mouse anti-GFP IgG



B. PAGE analysis

1. Coomassie blue staining



2. Coomassie blue then silver staining

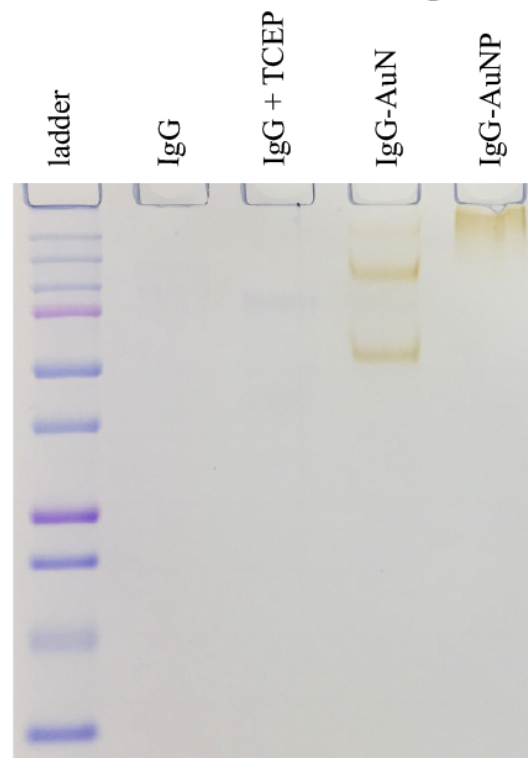
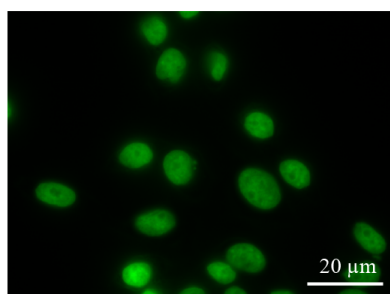


Figure S11. Preparation and analysis of the IgG-AuNP conjugate. A. Schematic route to the preparation of the anti-GFP-gold nanoparticle conjugate. The mouse antibody (clone GFP-2A3, IGBMC, Strasbourg) was incubated with 1 mM TCEP for 6 h. The raw mixture was then reacted for 12 hours with the TAB-, TNB- coated AuNP (1.5 equivalent). The conjugate was then purified by size exclusion (BioRad P100, elution PBS). The conjugate (IgG-AuN) was then reacted with thiolated PEG2000 (40 equivalents) for passivation of the remaining exchangeable TAB and TNB ligands onto the gold particle. The conjugate IgG-AuNP was purified again by size exclusion (BioRad P100) and concentrated by ultracentrifugation. B. PAGE analysis of the starting IgG and of the conjugates before and after passivation with thiolated PEG. The left image shows the gel after Coomassie blue staining to detect the protein. The right images (left) shows the Coomassie blue stained gel that was further treated with silver for the amplification of gold particles. Data showed effective conjugation both by detection of gold and by the observation of a fully retarded band when PEG was attached onto the AuNP surface.

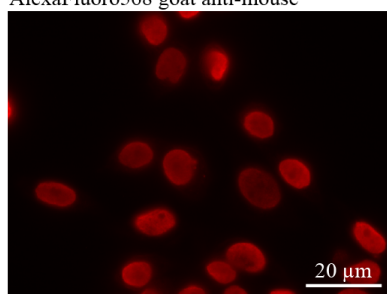
A. Immunodetection of the mouse anti-GFP antibody into the H2B-GFP HeLa



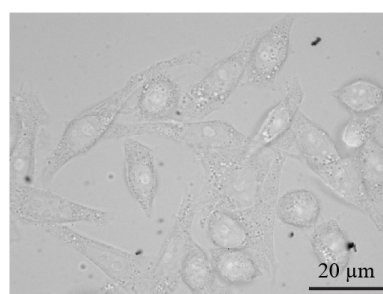
1. Detection of GFP



2. Detection of the secondary AlexaFluoro568 goat anti-mouse



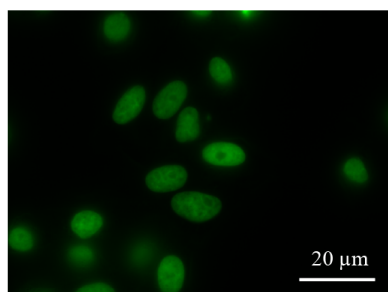
3. Silver enhancement IgG



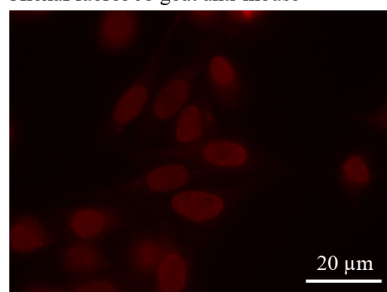
B. Immunodetection of the mouse anti-GFP antibody-AuNP conjugate



1. Detection of GFP



2. Detection of the secondary AlexaFluoro568 goat anti-mouse



3. Silver enhancement of the IgG bound AuNP

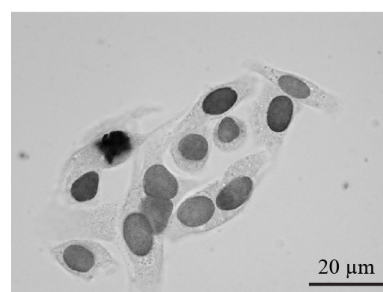
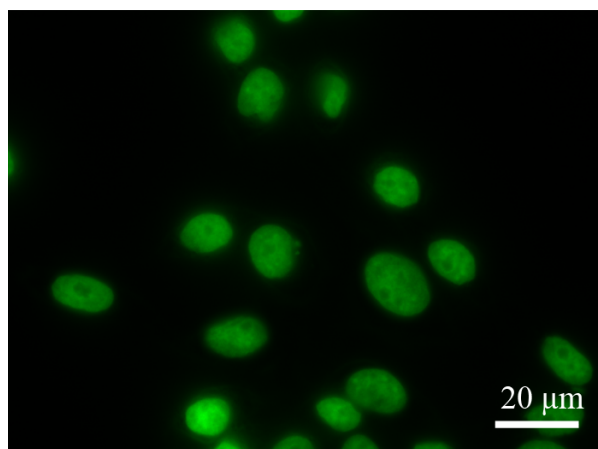
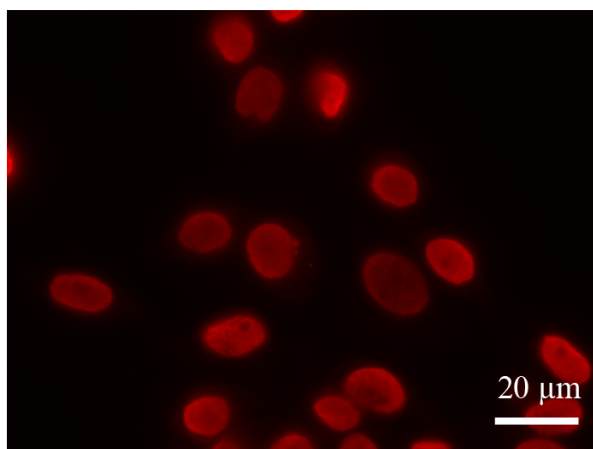


Figure S12. Fluorescent and silver-enhanced images of H2B-GFP HeLa cells after IgG and IgG-AuNP -mediated detection of GFP. The cells were fixed in 0.1M Sorenson buffer containing 4% PFA for 30 min and then permeabilization with 0.1% Triton X-100 in PBS. A. Immunodetection and silver enhancement of the mouse anti-GFP IgG (clone GFP-2A3) and of the corresponding AuNP conjugate were then performed using a secondary AlexaFluoro568 goat anti-mouse. B. Immunodetection and silver enhancement of the mouse anti-GFP IgG-AuNP conjugate. The permeabilized cells were incubated with 7 nM antibody or antibody conjugate in PBS containing 10% FBS.

Immunodetection of the anti-GFP mouse antibody into H2B-GFP HeLa cells

Detection of the GFP

Fixation: 4% PFA

Detection of the mouse anti-GFP
with a AlexaFluoro568 goat anti-mouse

Fixation: 2% PFA, 0.02 % glutaraldehyde

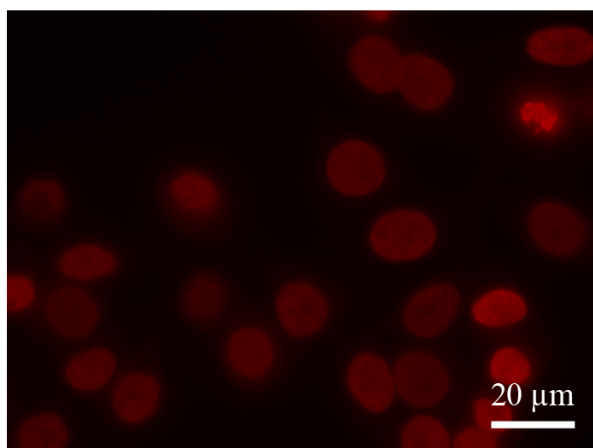
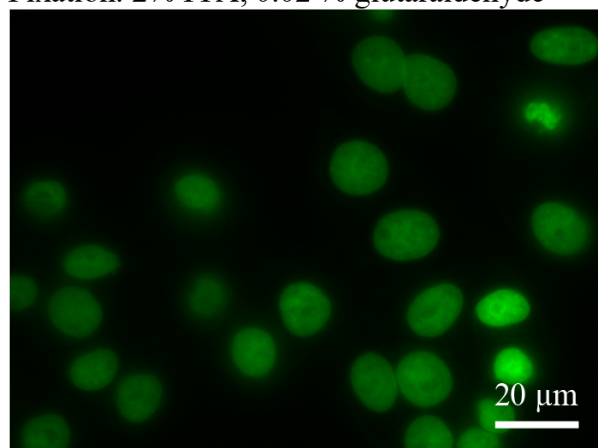


Figure S13. Fluorescent images of H2B-GFP HeLa cells after IgG-mediated detection of GFP. The cells were fixed in 0.2M HEPES buffer pH7.4 containing 4 % PFA or 2% PFA and 0.02% glutaraldehyde for 30 min. After permeabilization with 0.1% Triton X-100 in PBS (20 min), the GFP was bound by the mouse anti-GFP IgG (clone GFP-2A3, 7 nM in 10% FBS in PBS). After a washing step, the mouse anti GFP was detected with a secondary AlexaFluoro568 goat anti-mouse (7 nM).

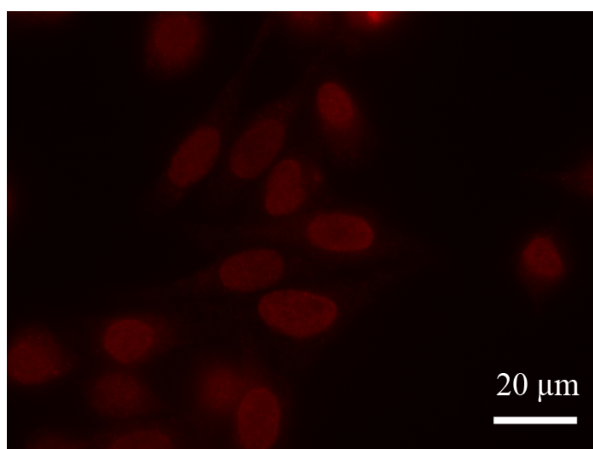
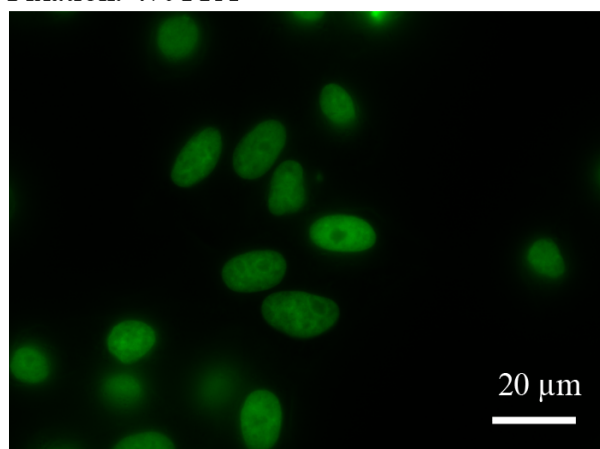
Immunodetection of the anti-GFP mouse antibody-AuNP conjugate into H2B-GFP HeLa

Detection of the GFP

Detection of the mouse anti-GFP

with a AlexaFluoro568 goat anti-mouse

Fixation: 4% PFA



Fixation: 2% PFA, 0.02 % glutaraldehyde

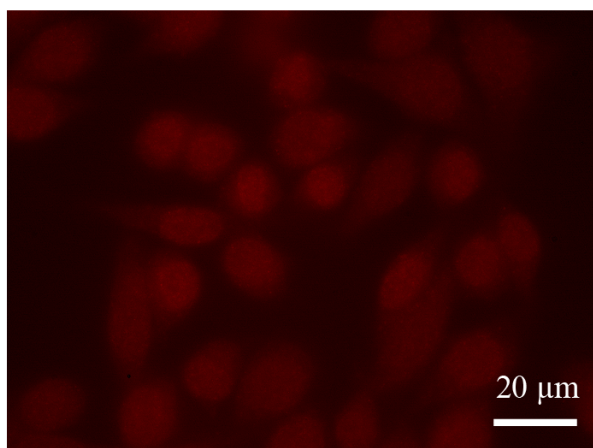
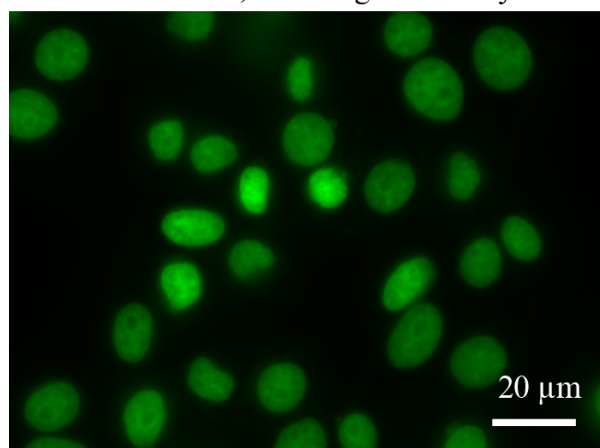
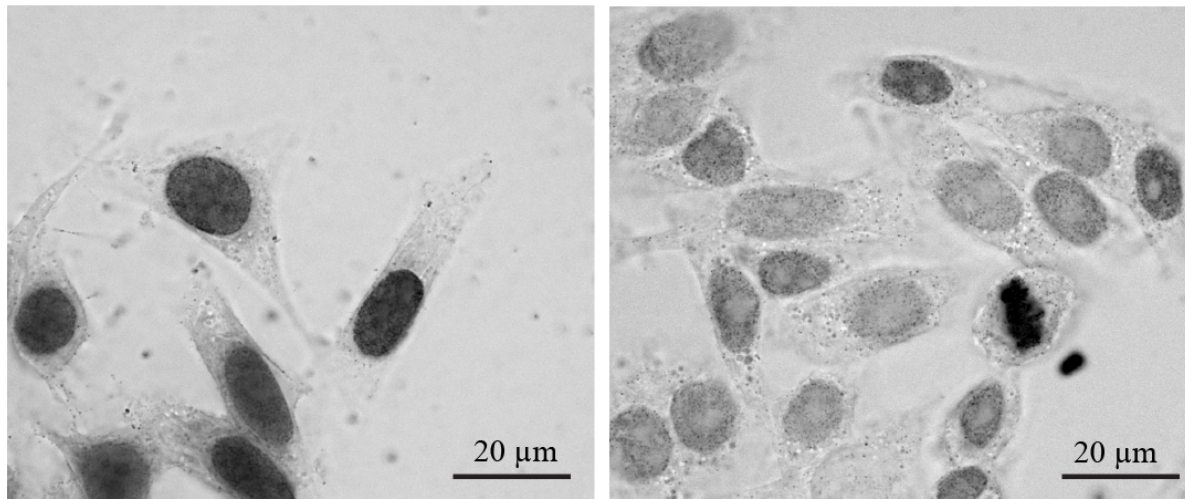


Figure S14. Fluorescent images of H2B-GFP HeLa cells after IgG-mediated detection of GFP. The cells were fixed in 0.2M HEPES buffer pH7.4 containing 4 % PFA or 2% PFA and 0.02% glutaraldehyde for 30 min. After permeabilization with 0.1% Triton X-100 in PBS (20 min), the GFP was bound by the mouse anti-GFP IgG-AuNP conjugate (7 nM in 10% FBS in PBS). After a washing step, the mouse anti GFP domain was detected with a secondary AlexaFluoro568 goat anti-mouse (7 nM).

1. $(\text{Nb-E})_2:(\text{K3})_2 \text{AuNP}$, 4 days storage at 4°C 2. $(\text{Nb-E})_2:(\text{K3})_2 \text{AuNP}$, 7 days storage at 4°C^*



3. $(\text{Nb-E})_2$, washing steps, then $(\text{K3})_2 \text{AuNP}$



Figure S15. Analysis of $(\text{Nb-E3})_2:(\text{K3})_2 \text{AuNP}$ ability to detect GFP into H2B-GFP HeLa cells several days after assembly and evaluation of the sequential immunogold labelling methodology. Images 1 and 2: the $(\text{Nb-E3})_2:(\text{K3})_2 \text{AuNP}$ was assembled by mixing the $(\text{Nb-E3})_2$ with $(\text{K3})_2 \text{AuNP}$ in PBS (final concentration $2 \mu\text{M}$). The assembly was then stored at 4°C for 4 and 7 days before being used as immunogold labelling marker at a 10 nM concentration. Image 3. The fixed and permeabilized H2B-GFP HeLa cells were incubated first with 10 nM $(\text{Nb-E3})_2$ in PBS containing 10% FBS and then with 10 mM $(\text{K3})_2 \text{AuNP}$. Before incubation with the labelling markers, the cells were fixed with 0.2 M HEPES pH 7.4 containing 4% PFA (30 min) and the cell membrane were permeabilized with 0.1% Triton X-100.

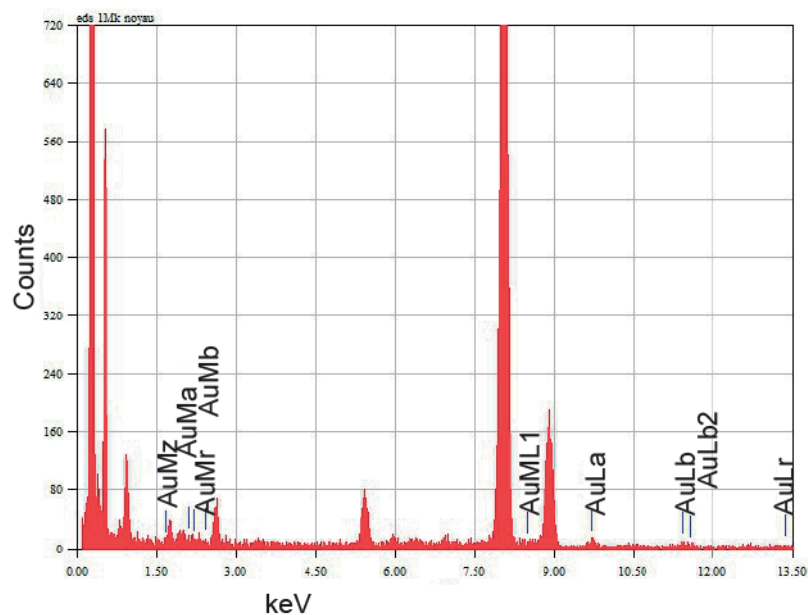


Figure S16. EDX spectroscopy analysis of a nuclear portion of H2B-GFP HeLa after gold immunolabeling with $(\text{Nb-E3})_2:(\text{K3})_2\text{AuNP}$ without silver-enhancement. The specimen was resin-embedded with the omission of the silver enhancement of the AuNP. The spectrum shows that the imaged nuclear area contains gold atoms. The intense peak at 0.277 keV is attributed to carbon and the intense peaks at 0.93 keV, 8.04 keV and 8.9 keV are attributed to copper, both resulting from the EM grids.

EDX spectroscopy analysis of a nuclear portion of H2B-GFP HeLa after gold immunolabeling with $(\text{Nb-E3})_2:(\text{K3})_2\text{AuNP}$ and silver-enhancement

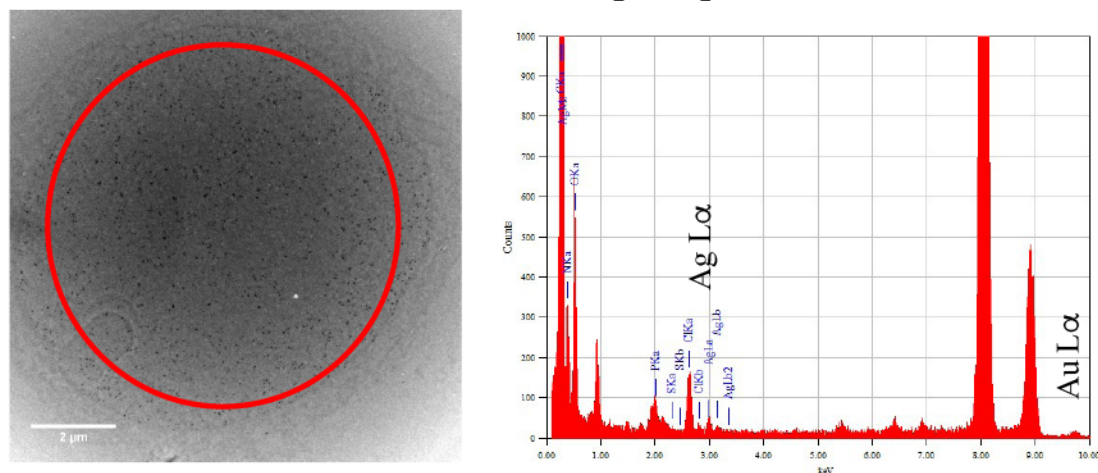


Figure S17. EDX spectroscopy analysis of nuclear portion of the H2B-GFP HeLa specimen after gold immunolabeling with $(\text{Nb-E3})_2:(\text{K3})_2\text{AuNPs}$ and silver enhancement. The spectrum indicate the presence of Au $L\alpha$ (9,712 eV) and Ag $L\alpha$ (2.984) signals suggesting that the silver deposition occurs on AuNP as claimed by Aurion, the manufacturer of the silver enhancement solution.

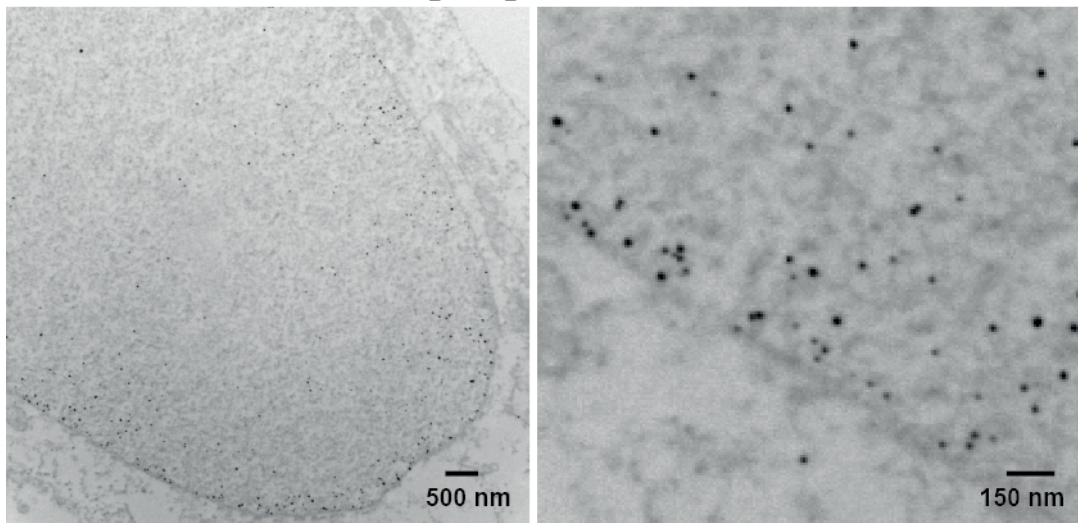
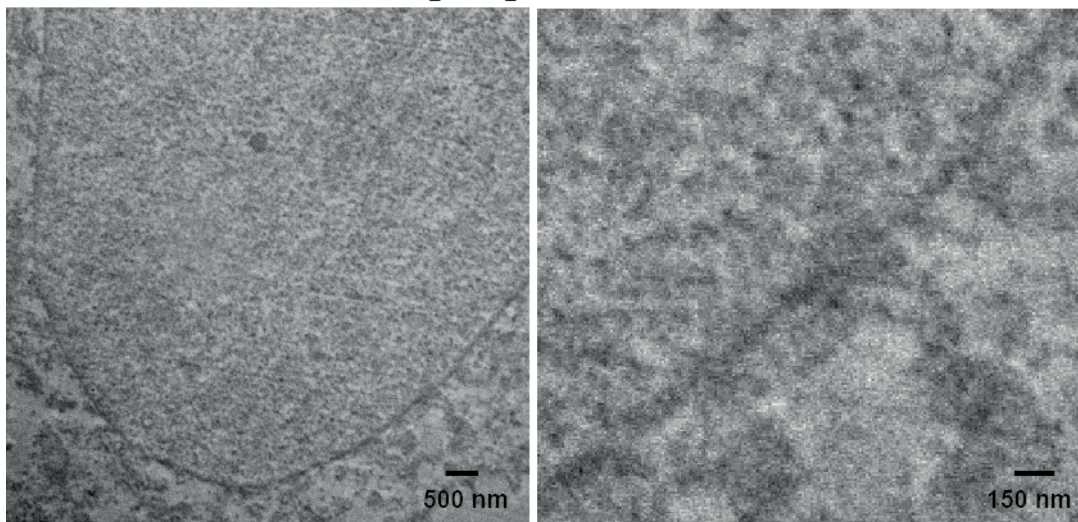
A. EM observation of $(\text{Nb-E3})_2:(\text{K3})_2\text{AuNP}$ labeled H2BGFP-HeLa**B. EM observation of $(\text{Nb-E3})_2:(\text{K3})_2\text{AuNP}$ labeled wild type HeLa**

Figure S18. Pre-embedding immuno-EM of the histone protein H2B-GFP with $(\text{Nb-E3})_2:(\text{K3})_2\text{AuNP}$. After immunolabeling and post-fixation, AuNPs were silver enhanced and membranes stained with OsO_4 . Labels were seen only in the nuclei of H2B-GFP HeLa cells and not in the nuclei of the wild type HeLa.

References

- 1 N. Groysbeck, A. Stoessel, M. Donzeau, E. C. da Silva, M. Lehmann, J.-M. Strub, S. Cianferani, K. Dembélé and G. Zuber, *Nanotechnology*, 2019, **30**, 184005.
- 2 X. Liu, M. Atwater, J. Wang and Q. Huo, *Colloids and Surfaces B: Biointerfaces*, 2007, **58**, 3–7.
- 3 D. Desplancq, N. Groysbeck, M. Chiper, E. Weiss, B. Frisch, J.-M. Strub, S. Cianferani, S. Zafeiratos, E. Moeglin, X. Holy, A. L. Favier, S. De Carlo, P. Schultz, D. Spehner and G. Zuber, *ACS Applied Nano Materials*, 2018, **1**, 4236–4246.
- 4 M. H. Kubala, O. Kovtun, K. Alexandrov and B. M. Collins, *Protein Science*, 2010, **19**, 2389–2401.
- 5 G. Freund, D. Desplancq, A. Stoessel, R. Weinsanto, A.-P. Sibling, G. Robin, P. Martineau, P. Didier, J. Wagner and E. Weiss, *J. Mol. Recognit.*, 2014, **27**, 549–558.
- 6 B. M. Humbel, M. D. de Jong, W. H. Müller and A. J. Verkleij, *Microsc. Res. Tech.*, 1998, **42**, 43–58.
- 7 C. Chandrashekar, B. Pons, C. D. Muller, N. Tounsi, R. Mulherkar and G. Zuber, *Acta Biomater*, 2013, **9**, 4985–4993.